Optimizing multiple non-invasive techniques (PXRF, pMS, IA) to characterize coarse-grained igneous rocks used as building stones

Antoine Triantafyllou, Nadine Mattielli, Sébastien Clerbois, Anne-Christine da Silva, Pim Kaskes, Philippe Claeys, Xavier Devleeschouwer, Gaël Brkojewitsch

Journal of Archaeological Science 129 (2021) 105376

Contents lists available at ScienceDirect

Journal of Archaeological Science

journal homepage: http://www.elsevier.com/locate/jas

Optimizing multiple non-invasive techniques (PXRF, pMS, IA) to characterize coarse-grained igneous rocks used as building stones

A. Triantafyllou [a,b,c,*], N. Mattielli [c], S. Clerbois [d], A.C. Da Silva [b], P. Kaskes [c,e], Ph Claeys [e], X. Devleeschouwer [f], G. Brkojewitsch [g,h]

[a] Geology Laboratory of Lyon - Earth, Planets and Environment (LGL-TPE), Université de Lyon, Université Lyon 1, ENS de Lyon, CNRS, UMR 5276, F-69622, Villeurbanne, France
[b] Department of Geology, Liège University, Sart Tilman, Liège, Belgium
[c] Laboratoire G-Time, Université Libre de Bruxelles, ULB, CP 160/02, Brussels, Belgium
[d] CReA-Patrimoine (Centre de Recherche en Archéologie et Patrimoine), Université Libre de Bruxelles, ULB, CP 133, Brussels, Belgium
[e] Analytical, Environmental and Geo-Chemistry, Vrije Universiteit Brussel, Pleinlaan 2, Brussels, 1050, Belgium
[f] Royal Belgian Institute of Natural Sciences, Geological Survey of Belgium, Brussels, 1000, Belgium
[g] Pôle Archéologie Préventive Metz-Métropole, Metz, France
[h] Centre Camille Jullian, UMR 7299, Aix-en-Provence, France

ARTICLE INFO

Keywords:
Geoarchaeology
Granite discrimination
PXRF
ML-Image segmentation
Magnetic susceptibility
Roman quarry

ABSTRACT

We present a workflow to conduct a full characterization of medium to coarse-grained igneous rocks, using portable, non-invasive, and reproducible approaches. This includes: *(i)* Image Analysis (IA) to quantify mineral phase proportions, grain size distribution using the Weka trainable machine learning algorithm. *(ii)* Portable X-ray fluorescence spectrometer (PXRF, Bruker Tracer IV) to quantify the whole-rock's chemical composition. For this purpose, a specific calibration method dedicated to igneous rocks using the open-source CloudCal app was developed. It was then validated for several key elements (Si, Al, K, Ti, Ca, Fe, Mn, Sr, Ga, Ba, Rb, Zn, Nb, Zr, and Y) by analyzing certified standard reference igneous rocks. *(iii)* Portable Magnetic Susceptibilimeter (pMS, Bartington MS2K system) to constrain the mineralogical contribution of the samples. The operational conditions for these three methods were tested and optimized by analyzing five unprepared surfaces of igneous rocks ranging from a coarse-grained alkaline granite to a fine-grained porphyric diorite and hence, covering variable grain sizes, mineralogical contents, and whole-rock geochemical compositions. For pMS and PXRF tools, one hundred analyses were conducted as a 10 cm × 10 cm square grid on each sample. Bootstrap analysis was implemented to establish the best grid size sampling to reach an optimized reproducibility of the whole-rock signature. For PXRF analysis, averaged compositions were compared to PXRF analysis on press-pellets and laboratory WD-XRF analysis on fused disk and solution ICP-OES (for major) and solution-ICPMS (for trace element concentrations). Ultimately, this workflow was applied in the field on granitoids from three Roman quarrying sites in the Lavezzi archipelago (southern Corsica) and tested against the Bonifacio granitic War Memorial, for which its provenance is established. Our results confirm this information and open the door to geoarchaeological provenance studies with a high spatial resolution.

1. Introduction

One of the main challenges in archaeometry and geoarchaeological studies is to develop versatile, non-invasive, and efficient analytical tools that constrain the provenance of onsite archeological materials (Bersani and Lottici, 2016; Killick et al., 2020; Mathur et al., 2020; Liritzis et al., 2020 and references therein). Linking pieces of tools, artifacts, monuments, building elements, etc. With their extraction and production site brings crucial information on the extension of former commercial trades as well as the nature and modes of these exchanges and the transportation of raw materials (e.g., Williams-Thorpe, 2008; Vandenabeele and Donais, 2016; Fantuzzi et al., 2020). The last decades

* Corresponding author. Geology Laboratory of Lyon - Earth, Planets and Environment (LGL-TPE), Université de Lyon, Université Lyon 1, ENS de Lyon, CNRS, UMR 5276, F-69622, Villeurbanne, France.
E-mail address: antoine.triantafyllou@univ-lyon1.fr (A. Triantafyllou).

https://doi.org/10.1016/j.jas.2021.105376
Received 19 January 2021; Received in revised form 16 March 2021; Accepted 17 March 2021
Available online 6 April 2021

have seen tremendous developments of non-invasive analytical techniques with increased enhancements in portability and data accuracy. These technological advances were boosted by geological exploration and mining prospection (e.g., Fabre, 2020), environmental studies (e.g., Turner et al., 2018), and/or planetary rover missions (Edwards, 2018), along with many other applications. Specifically, in archaeometry, more and more non-destructive tools in spectroscopy and spectrometry are used to constrain the mineralogy, the chemical composition, and the physical properties of archeological material, by e.g., portable magnetic susceptibility (pMS; e.g., Williams-Thorpe and Potts, 2002; Szakmány et al., 2011), portable XRF (Oyedotun, 2018; Müskens et al., 2018; Sinnesael et al., 2018), portable Gamma-Ray spectrometry (pGRS; Puccini et al., 2014), handheld Laser-Induced Breakdown Spectroscopy (HH-LIBS; Senesi et al., 2018), portable Raman spectroscopy (e.g., Bersani and Madariaga, 2012) or spectrophotometry (Rogerio-Candelera, 2016; Boulvain et al., 2020). Combining these tools and the interpretation opens the door to high accuracy determination, discrimination, and sourcing of archeological materials (e.g., Liritzis and Zacharias, 2011; Papakosta et al., 2020).

Nevertheless, and to the best of our knowledge, studies using these tools were generally applied individually and/or for analyzing homogeneous and fine-grained materials; *i.e.,* aphanitic or vitreous volcanic rocks (e.g., obsidian, andesite; Williams-Thorpe et al. 1999; Steiner et al., 2017; Burke, 2018; Germinario et al., 2018), sedimentary-related rocks and their host units (silex, marbles, etc.; Kasztovszky et al., 2018; Clinton et al., 2019), metallic alloys (Karydas, 2007) and/or bricks and ceramics pottery manufactured mixing fine-grained soils, metallic elements and/or rock powders (e.g., Bonizzoni et al., 2013; Hunt and Speakman, 2015; Baziotis et al., 2020; Eramo and Mangone, 2020). However, such non-invasive and handheld approaches are less explored to characterize medium to coarse grained igneous rocks, for which grain size indeed implies analytical challenges and complexifies the instrumental signal interpretations (Lemiere, 2018). Besides, the quantification of chemical element contents, using PXRF for example, strongly depends on the calibration strategy and the use of matrix-match reference materials to build it. If inappropriate, a given PXRF instrument can provide irrelevant and/or non-reproducible results (Hunt and Speakman, 2015). Manufacturers' pre-loaded instrument calibrations can help comparing the chemical composition of a given sample material with a specific matrix, analyzed with the same instrument, with constrained environmental conditions (lab, field, etc.). This approach can be a source of error for case studies using different PXRF tools and under other analytical and environmental conditions (Hall et al., 2014). These considerations can constitute a significant impediment to integrated/review studies from collaborative research programs and literature data compilations (Craig et al., 2007).

Coarse-grained igneous rocks, granitoids *sensu lato*, were a widespread element in Rome's architecture since the Imperial era (Galetti et al., 1992). These rock types were intensively quarried to provide monumental, durable and elegant architectural pieces (e.g., columns, fronton, arches, obelisks; Adam, 2011) that were ultimately used to build colossal edifices in the entire Mediterranean basin (see Waters, 2016 and references therein). Sourcing these granitic monuments still provide crucial information to constrain quarrying strategies, the dynamics of raw materials transportation and vectors of commercial trades through the empire (Williams-Thorpe, 2008; Clerbois et al., 2020). Addressing these questions requires developing and validating analytical methods using non-invasive, non-destructive, and portable instruments.

Therefore, this study presents a workflow that combines three non-destructive and handheld techniques (PXRF, pMS, and image analysis) to perform the characterization of fine to coarse grained igneous rocks. We firstly selected five in-house and well-characterized granitoids, which cover the diversity of granitoid grain sizes and chemical compositions. A detailed lab characterization was performed on these reference materials with the three non-invasive methods. We explore the advantages and limitations of different quantification approaches; the effect of operational conditions and rock grain size to finally propose an optimized and calibrated protocol based on these three techniques. Secondly, we illustrate and validate our methodology by investigating Roman quarrying activities in the Lavezzi archipelago (southern Corsica, in the Straits of Bonifacio). The geochemical signature of granitic rocks extracted from each island's quarry (*i.e.* two quarries combined on Lavezzu, one on Cavallo, and one on San Bainzu islands) is compared with the one of a monumental column exposed in the Bonifacio locality. The latter is well documented, and thus, its origin can be tested against our archaeometric methodology. The three quarrying sites are not distant from each other (<5 km). They exploit a relatively homogeneous pluton and are thought to provide comparable granitoids' products, difficult to distinguish for human eyes between each other. Our study shows that combining multiple proxies from non-destructive and well-calibrated techniques allows us to discriminate them. Hence, it is a crucial approach to identify provenances with a high spatial resolution. We ultimately discuss some promising perspectives and their applicability in geoarchaeological and solid rock geological investigations.

2. Materials and workflow description

Five samples of granitoids were selected from in-house rock collection based on their freshness and their variability in grain size, along with their variations in Fe–Mg- and alkali-rich phases. From coarse to fine-grained samples, our working set is made of: (1) a pink coarse-grained granite from Ploumanac'h (Brittany, western France, hereafter: PLOU), (2) a leucocratic coarse-grained granite (Tarn region, southern France, hereafter: TARN), (3) a coarse to medium-grained granite (Galicia, Spain, hereafter: GAL), (4) a medium-grained leucogranite (Ariège, Pyrenees, southern France, hereafter: RGR) and (5) a fine-grained porphyric reddish granodiorite (Quenast intrusion, Belgium, hereafter: QUE). Each rock block was cut into two pieces: one of the faces was finely polished using up to 5 μm abrasive diamond powder solution (before being cleaned with methanol). A 10 × 10 cm squared area was drawn on the polished face (with a 1 cm spaced grid), ensuring a representative area (*i.e.*, in texture, mineralogy, and grain size) of each of the fine to coarse-grained samples. Non-destructive analyses, using image analysis (IA; section 3), portable X-ray energy dispersive Fluorescence spectrometer (section 4), and portable magnetic susceptibility meter (pMS; section 5) were conducted similarly for the five rock samples and for the 100 points of the grid. An aliquot of each granitic rock was extracted from the other rock face, finely powdered using agate jars for destructive chemical analysis using WD-XRF, ICP-OES (for major chemical elements) and solution ICP-MS (for trace elements; see section 4.3). These complementary approaches will provide reliable and precise whole-rock chemical analyses for each of investigated granitic rocks used to optimize and validate the non-destructive approaches.

3. Quantitative image analysis

3.1. Image acquisition and processing

The 10 × 10 cm area of the five granitoids was imaged using a digital field camera (Nikon D5300 DSLR) and sunshine/natural lighting. A reference color chart was shot preliminary to correct RAW images for white balance, color accuracy, and tonal response under given lighting conditions. Each RAW image was then cropped, converted, and exported as a JPEG file (see Fig. 1a). These images were then imported into the Fiji-ImageJ app (Schindelin et al., 2012), scaled, and enhanced (for contrast and exposure). Images were then segmented for each phase (minerals or groundmass) distinguished on the macroscopic sample, using the Weka trainable machine-learning (ML) algorithm in Fiji-ImageJ (Arganda-Carreras et al., 2017; see Fig. 1b for the TARN sample). Phases proportion was then computed and exported using

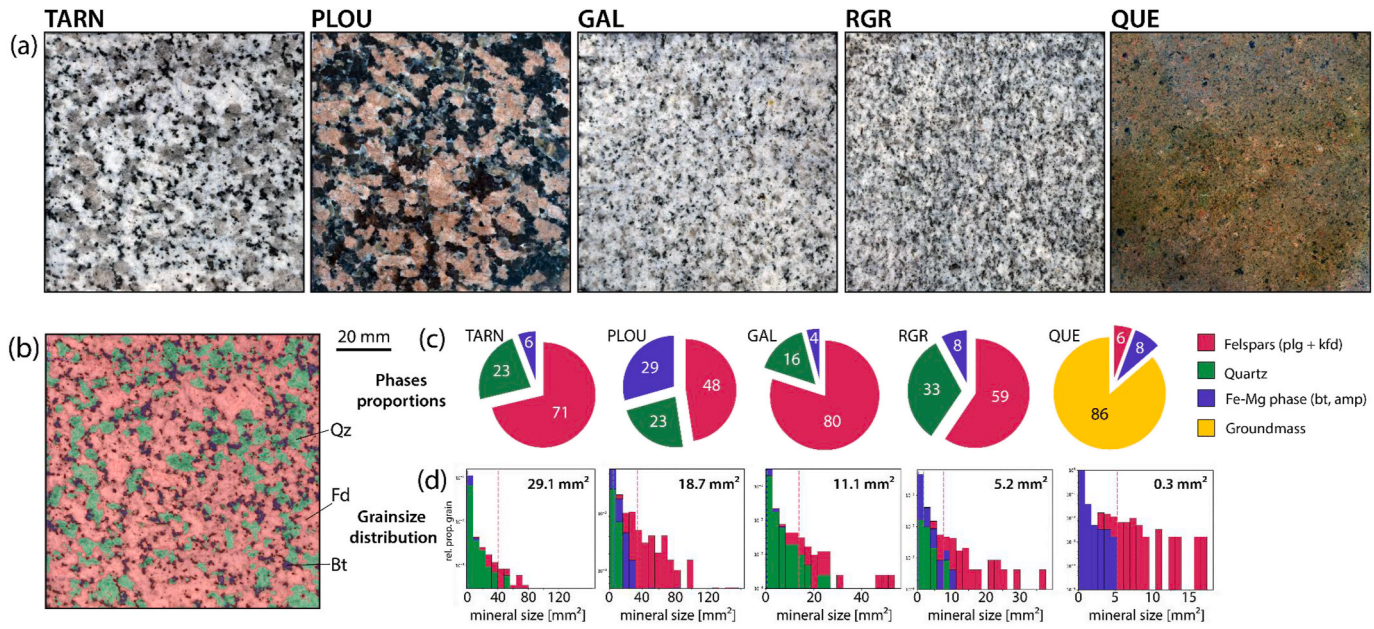

Fig. 1. Image analysis on in-house reference materials. (a) Images of polished surface for each sample. (b) Results of image segmentation using Weka trainable machine learning algorithm. (c) Pie chart showing phases proportions for each igneous rock. (d) Stacked histogram plots showing grainsize distribution in igneous rock samples and weighted median value of grains size quantifying large to low grainsize from left to right. Fd is for felspar, Qz for quartz and Bt for biotite. (Figure orientation: use landscape for easy reading).

ImageJ Measurement Tool and grain size distribution using SPO software (Launeau et al., 1990). Each mineral's surface area in 2D was considered representative of each phase's volume (%vol in the next section).

3.2. Results for quantitative image analysis

Results for phase proportions and weighted average grain size per mineral are summarized in Fig. 1 c-d and full results can be found in Appendix A1. Whole-rock grain size (defined as weighting average of each mineral phase's grain size using their modal proportion) is expressed in mm^2 and ranges from 29.1 mm^2 in TARN sample (coarse-grained granite) to 0.3 mm^2 in QUE sample (porphyric microdiorite). Phase proportions are grouped as follows: feldspars (including plagioclase plus K-felspar that cannot efficiently be distinguished using macroscopic image analysis), quartz, ferromagnesian phases (including biotite, amphibole) and the fine-grained groundmass (only for QUE sample and its porphyric texture; Fig. 1a). Phase proportions results range from 6 to 80 vol % in felspar for the GAL leucogranite and QUE subvolcanic diorite, respectively. PLOU granite shows the highest ferromagnesian mineral proportion (29 vol %) and RGR granite the highest quartz proportion (33 vol %).

4. Portable energy dispersive X-ray fluorescence spectrometer (PXRF)

4.1. Instrumental and operational conditions

Eighteen elements (Al, Si, K, Ti, Ca, Fe, Mg, Mn, Cu, Sr, Ga, Ba, Rb, Zn, Nb, Zr, Y, Cr) were chosen to be quantified using a Bruker Tracer IV® handheld PXRF device (from the Analytical, Environmental and Geo-Chemistry, Vrije Universiteit Brussel). This PXRF is equipped with a 2 W Rh anode X-ray tube, an 8 μm Be window and a Peltier-cooled ten mm^2 SSD (Silicon Drift Detector) with a resolution of 145 eV (Mn-Ka; de Winter et al., 2017). This PXRF is also equipped with a metallic cap and an Ultralene™ non-vacuum window (thin film) to protect the detector from dust during field investigation. No specific filter, collimator or vacuum systems was used in this study to be more versatile and cover a maximum of chemical elements. The irradiated area has a factory size of 8 × 10 mm during each analysis. The same conditions of illumination of the standard factory "*Soil Fundamental Parameters*" method, called "Soil calibration method" hereafter, was used (*i.e.* 45 kV and 30 μA) for the analyses of in-house granitoids, of certified standard reference materials (press pellets) as well as field igneous samples.

4.2. PXRF calibration and chemical validation

Press-pellets of standard reference material (SRMs) fine powders were prepared, mixing 5 g of rock powder with 2 mL of methyl methacrylate resin (Elvacite®) as a binding agent. The mixture was then pressed (200 kN/cm^2) for about 60 s. Preliminary PXRF chemical analyses on these SRMs (used as known unknowns) showed that the Soil calibration method for the Tracer IV could not provide concentrations accurate enough for the igneous matrix (see comparisons in next sections). We therefore extracted raw ED (Energy Dispersive) PXRF spectra to develop and generate an in-house empirical calibration method dedicated to igneous rocks. For this purpose, a set of twelve SRMs' pressed pellets (BEN, BHVO, BR, DRN, GSP-1, GSR-2, GSR-3, JA-1, JB-1b, JB-2, MAN, NIM-G) with compositions ranging from basalt to rhyolite were analyzed and processed in the open-source CloudCal app (2020 July version; Drake, 2019). Certified concentrations for major and trace elements can be found on the GeoReM database and GGR Review (Jochum et al., 2005, 2014). Each pressed pellet was analyzed for 75 s, as recommended in de Winter et al. (2017), with the same source and sensor conditions mentioned above. The raw spectra (PDZ filetype) of the first dataset were converted to CSV filetype using S1PXRF software (www.bruker.com). X-ray spectra were then imported into the CloudCal app. For each element, a region of interest (ROI) where to find the ED peak of interest was preliminary adjusted. A calibration curve was then generated for each chemical element using non-linear regression and the Lucas-Tooth and Price equation regression models (see procedure details in Sapkota et al., 2020a ,b). The quality of the calibration process and regression line equations are summarized in appendix A2 along with interference corrections, amount of omitted SRMs (being outliers in the calibration curves) and Compton normalization range used for each element peak energy. Most chemical elements showed promising

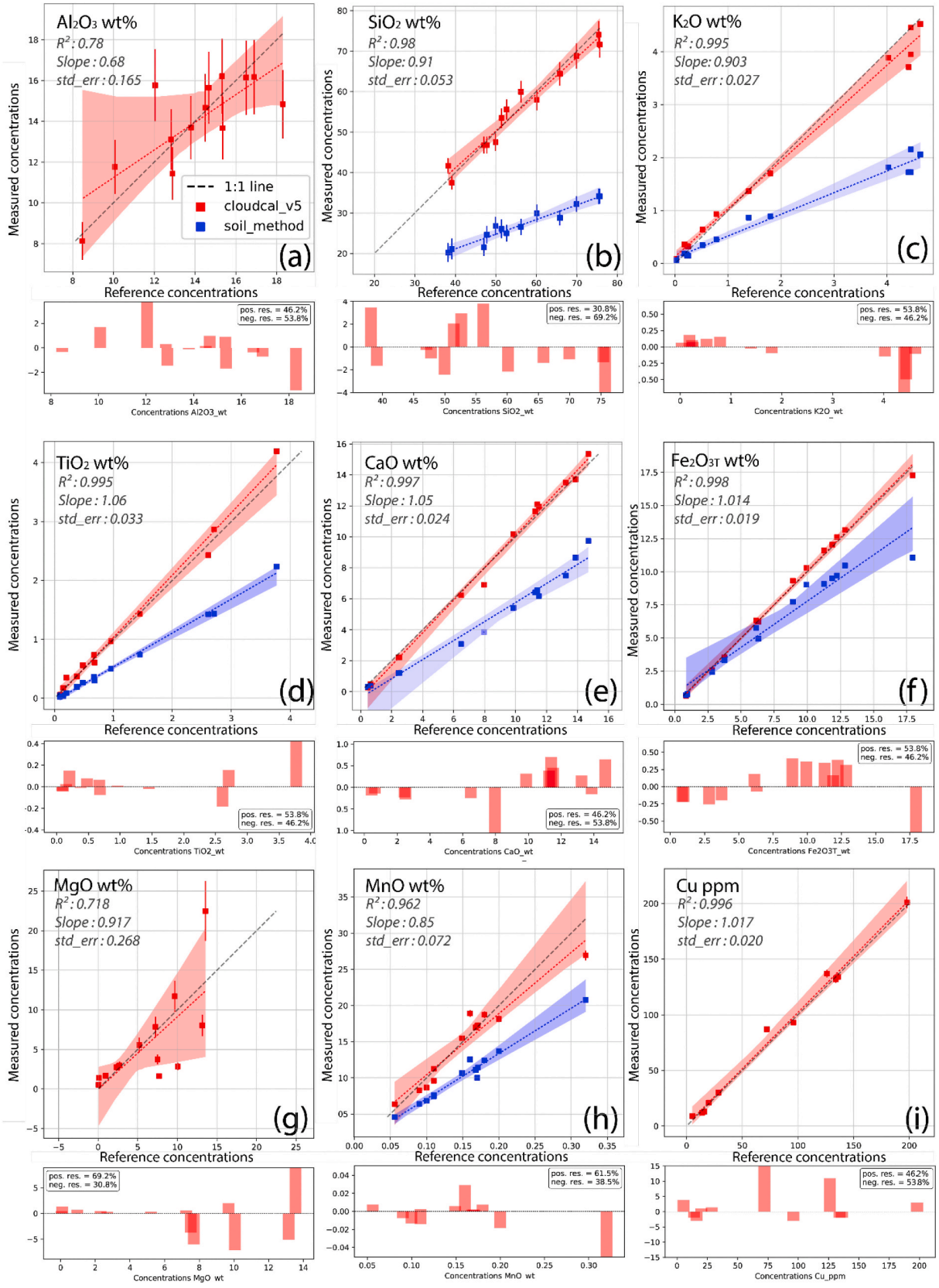

Fig. 2. External validation to evaluate our PXRF calibration, comparing measured vs reference concentrations of the SRMs press-pellets of igneous rocks (n = 12) analyzed as known-unknowns (see text for details). The dotted black line represents the expected 1:1 ratio between X-ray fluorescence (XRF) estimates and known concentrations. The dotted colored lines are the regression lines based on quantified mass fractions. Red and blue data are produced using our empirical calibration and the Bruker Soil method calibration, respectively. Some elements do not show blue regression lines as they are not quantified in the Soil calibration method. Histograms below each scatter plot show the distribution of the residuals compared the concentrations of used certified SRMs. (For interpretation of the references to color in this figure legend, the reader is referred to the Web version of this article.)

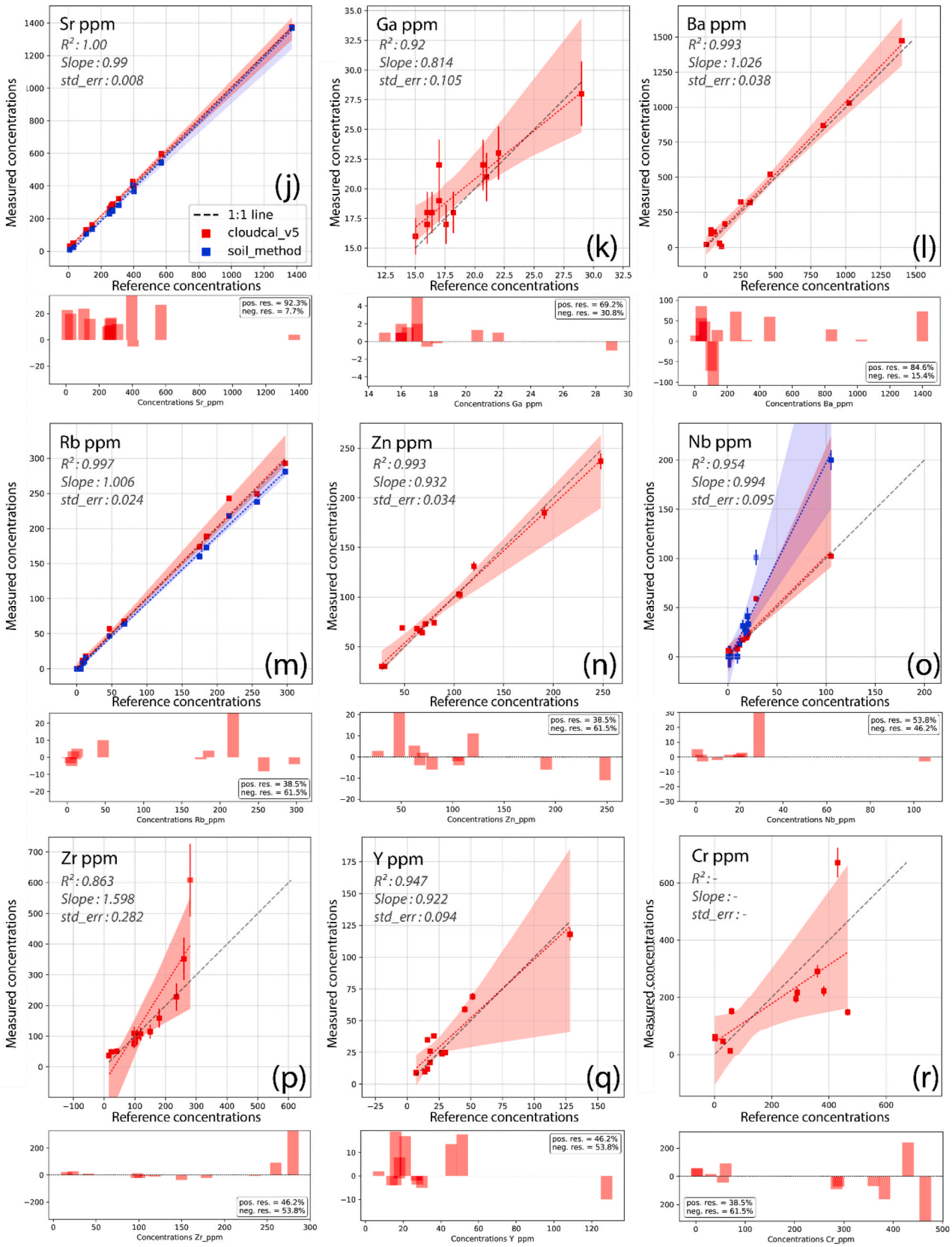

Fig. 2. (*continued*).

calibration curves except for V, Cr and As; hence, the latter was removed from the calibration method.

A subset of twelve additional SRMs' press-pellets (except for BHVO) of igneous rocks was then analyzed as known-unknowns (BIR, DNC-1, GA, GSN, BHVO-1, JA-2, JB-3, JR-1, JR-2, MRG-1, NIM-N, SY-2; see the GeoReM database for certified compositions) to validate our

calibration method (Fig. 2 a-r). Reference composition and quantified results are compared and show a good correlation (close to 1:1 line in Fig. 2) for most chemical elements. We used the determination coefficient (R^2), the slope value, and standard errors to characterize the quality of each element's regression line (see appendix A3 for a summary). Three chemical elements (Mg, Al and Zr) show > 10% of std error with low R^2 values (<86%); five other elements (Si, Mn, Ga, Y, Nb) are characterized by 5 and 10% of std error with moderate R^2 values (ranging between 92 and 98%) and the nine others (K, Ca, Ti, Fe, Cu, Zn, Rb, Sr, Ba) with <5% of std error with highest R^2 (>99.3%).

4.3. Chemical analyses by lab WD-XRF, solution-ICP-OES and -ICPMS

Reference geochemical compositions for major and trace elements were obtained through laboratory instruments for each of our five in-house granitoid samples (the same ones used for image analysis in section 3). Rocks were crushed and milled in agate jars. For major elements, about 0.5 g of rock powder has been mixed with lithium tetraborate (10:1) and ignited at 1000 °C for 2 h. Glass disks were then made in a platinum mold and analyzed using a laboratory X-ray fluorescence (XRF) spectrometer ARL PERFORM-X 4200 (Rh X-ray tube) at the University of Liège (Belgium). Detailed procedure and calibration method can be found in Vander Auwera et al. (2019). Bulk rock major element analyses were also performed on an iCAP™ 7400 ICP-OES Analyzer (Thermo Fisher Scientific), as well as trace elements analyzed with an Agilent 7700 quadrupole ICP-MS, both at the G-Time laboratory (Université Libre de Bruxelles, Belgium). A subsample of 0.05 g of rock powder was taken and mixed with 0.8 g of lithium metaborate and 0.2 g of lithium tetraborate in a graphite crucible. The crucible was then placed in a magnetic induction furnace to reach 1000 °C gradually, a temperature maintained for 5–10 min. The resulting glass disk was then transferred into a specific volume of 2 M HNO_3 nitric acid. After centrifugation and calculation of adapted dilutions, an aliquot is used for the ICP-OES analyses. External Standard Solutions were prepared from mono-elemental solutions of Silicon (Si), Magnesium (Mg), Iron (Fe), Aluminum (Al), Calcium (Ca), Sodium (Na), Titanium (Ti), Potassium (K), Phosphorus (P), Manganese (Mn) and Chromium (Cr), characterized by well-known contents for calibrating analyses on i-Cap. A Yb solution was added to the external standards and samples as an internal standard for corrections of the ICP-OES instrumental drift and matrix effects. Another aliquot of each sample was also prepared in 5% HNO3 before the ICP-MS analyses conducted using a He collision cell. Mono-elemental standard solutions were prepared to determine calibration lines for all elements to be analyzed. An indium solution was added to the sample, standard and blank solutions, and used as an internal standard. Standards Reference Materials BHVO-2 and BCR-2 were used as external calibration. Geochemical results for each granitoid sample can be found in Appendix A4.

4.4. PXRF chemical analysis of igneous rocks with different grain sizes

The calibration method and the influence of rock grain size were investigated using the five in-house granitoids samples. One hundred PXRF analyses were conducted row by row following the 10 × 10 cm (1 cm spaced) grid on the polished surface. It was done using the same protocol and illumination conditions described above (75 s analyses in FP Soil Mode: 45 kV, 3 μA for the source conditions). All the raw spectra were quantified using our dedicated CloudCal calibration (see examples of chemical mapping in Figs. 3 and 4 for SiO_2 and K_2O contents in wt%).

To investigate the impact of subsampling size, a bootstrap analysis (iterations = 1000) was conducted for each sample by subsampling n x n analyses (for n = 2, 3, 4, 5, 6) from the set of hundred analyses at each bootstrap iteration. Three different subsampling approaches were tested: firstly, by averaging n x n numbers of individual analyses sampled randomly (Fig. 5a), secondly by averaging n x n numbers of individual analyses that were sampled as a grid (of n x n size; Fig. 5b) and thirdly, by averaging the n x n raw spectra of a continuous subsampled grid (of n x n size) and by quantifying the elements' concentrations based using the averaged spectrum (Fig. 5c). The mean values distribution is shown for each subsampling method on Fig. 5 d-f (for the

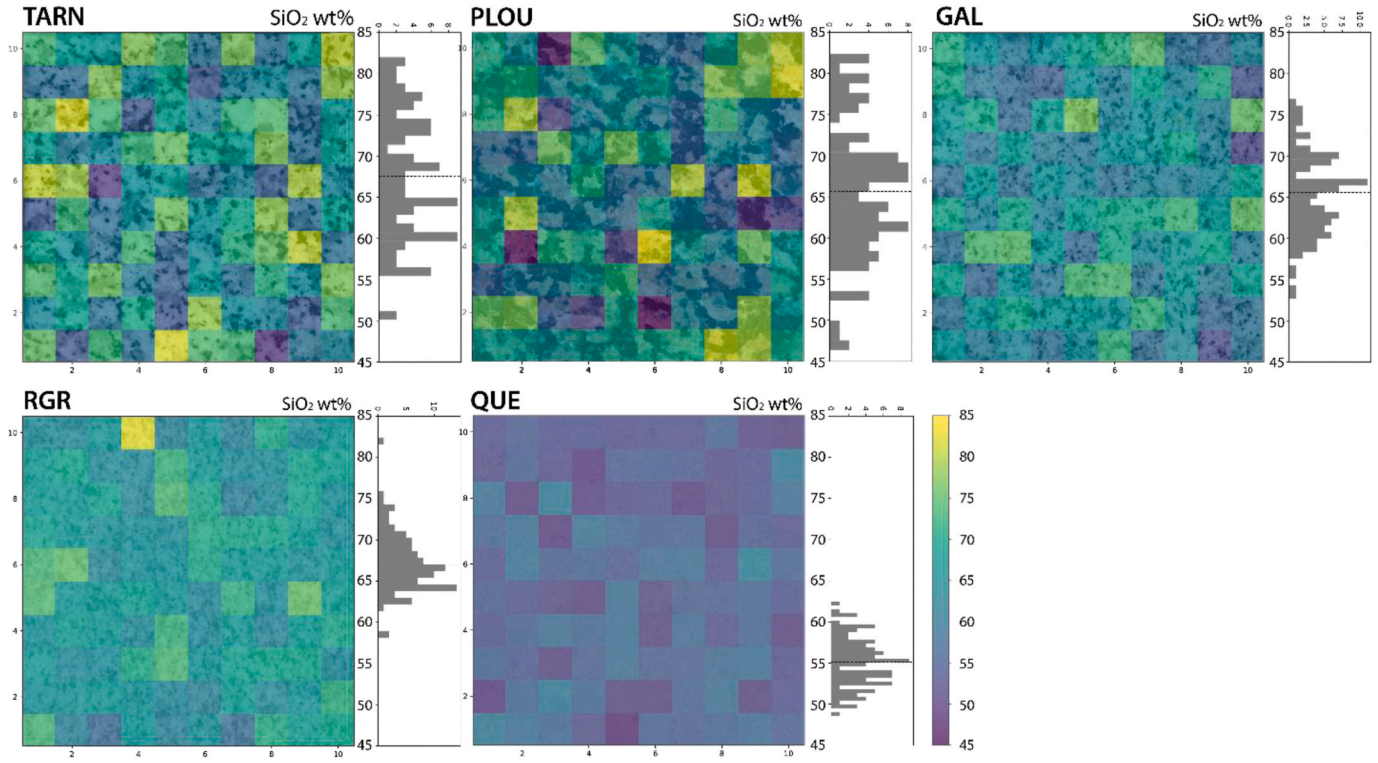

Fig. 3. SiO_2 wt% chemical mapping (10 × 10 PXRF analyses) for each sample of granitoid samples. Individual chemical analyses show large spread in relative abundance, reflecting the mineral phase and the grainsize distribution of each rock sample.

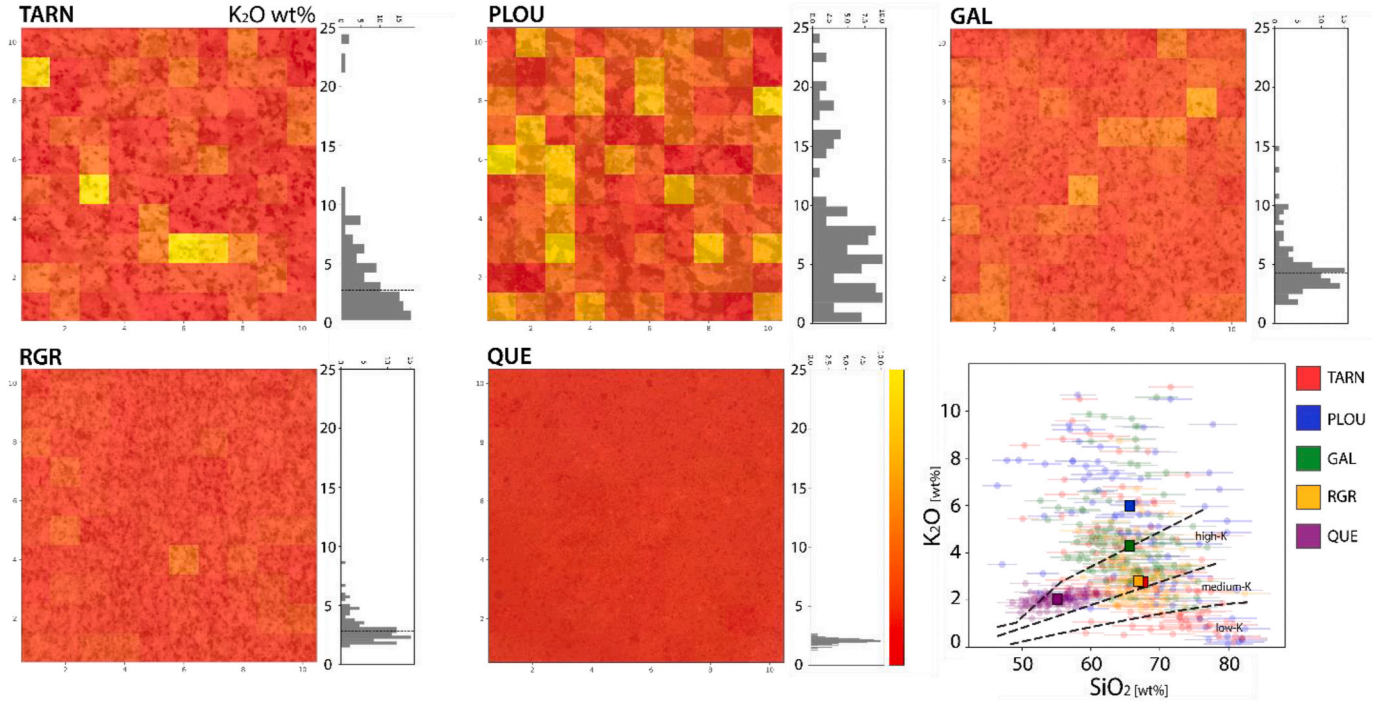

Fig. 4. K_2O wt% chemical mapping (10 × 10 PXRF analyses) for each polished surface of granitoid samples. In the bottom right corner, the scatter plot displays individual analyses (in transparency in the background) and their averaged composition in front. Their averaged compositions show that most of analyzed granitoids have a medium-to high-K signature.

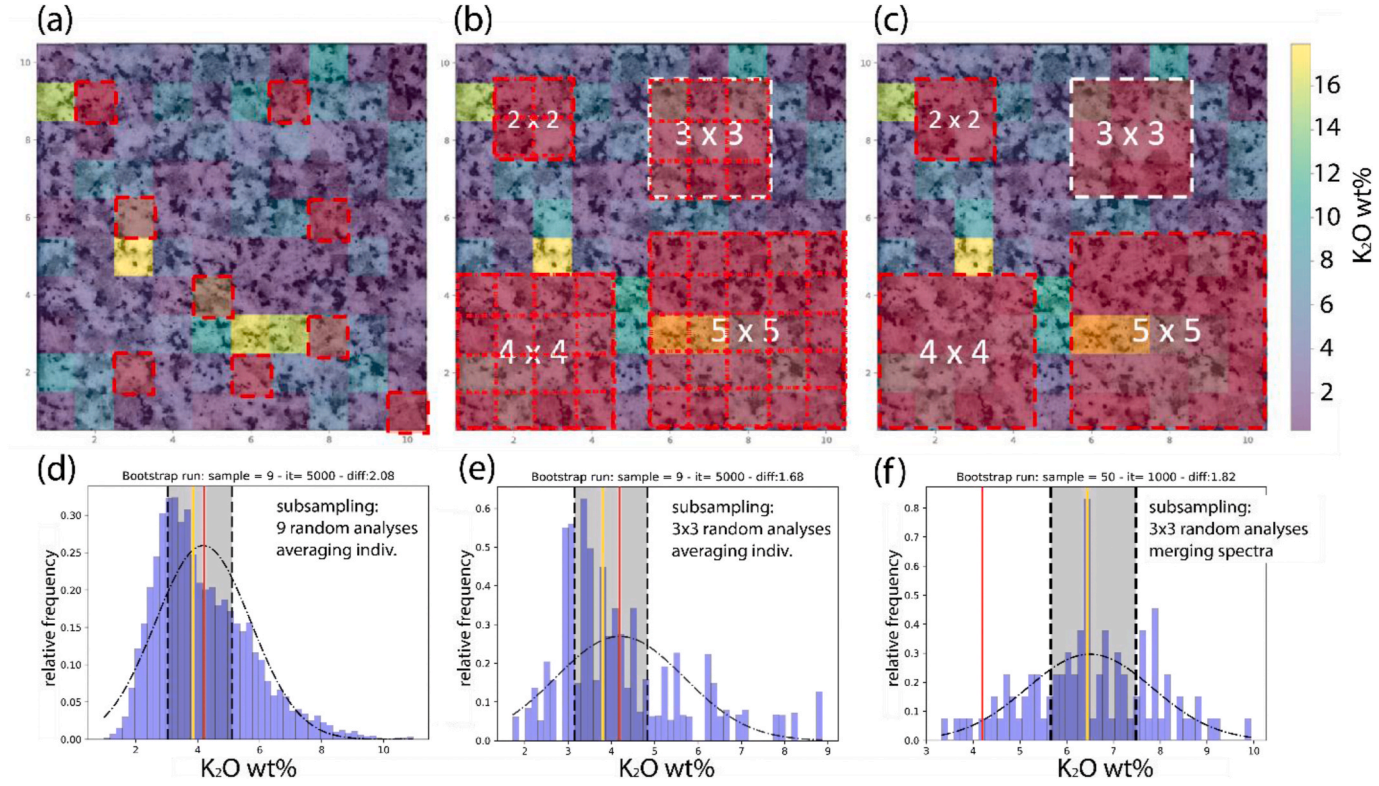

Fig. 5. Example of subsampling approaches illustrated here for the TARN coarse grained granite. (a) 9 random analyses in the K_2O map. (b) Squared subsampling of 4, 9, 16 and 25 analyses but quantifying each analysis individually and averaging quantified results. (c) Squared subsampling of 4, 9, 16 and 25 analyses but averaging each group of spectra and quantifying the averaged spectrum then. Distribution histogram of mean values by averaging n x n numbers of individual analyses picked randomly (d), by averaging n x n numbers of individual analyses that were sampled as a continuous grid (e), by averaging the n x n raw spectra of a given subsampled grid (of n x n size) and calculating the elements concentration based on the averaged spectrum (f). Vertical red line consists of WD-XRF concentration for comparison; yellow line is for the median value and dashed black lines are for 0.25 et 0.75 quantile values of the distribution. (For interpretation of the references to color in this figure legend, the reader is referred to the Web version of this article.)

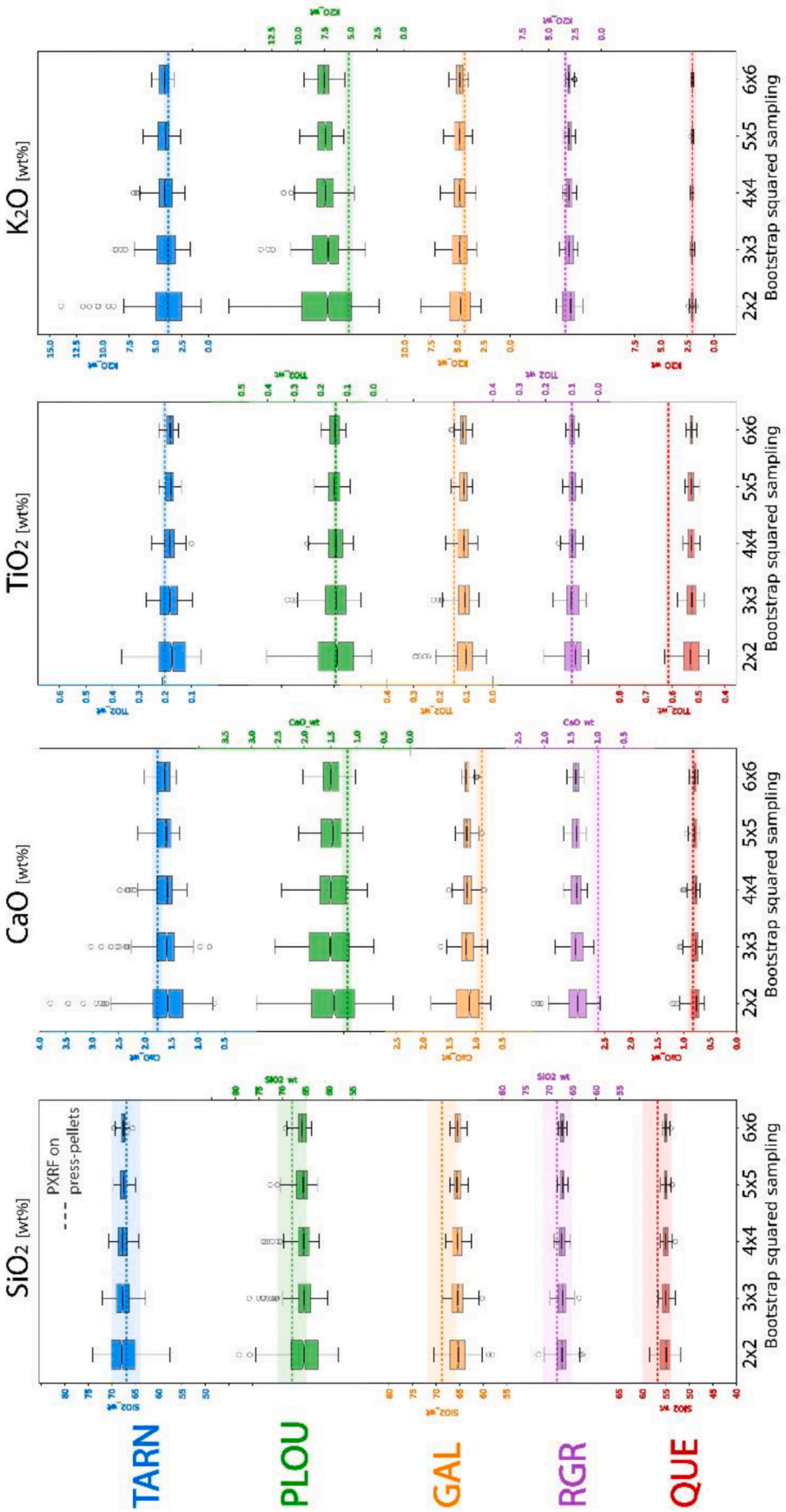

Fig. 6. Box plots showing the effect of square sampling size for PXRF analysis (using bootstrap iterations; n = 1000). Each sample was quantified, and elements concentrations averaged. Boxes extend from the lower to upper quartile values of each sampling size and the black line is for the median value. Black whiskers show the range of the dataset except for identified outliers in whitish round symbols. Dashed lines show single analysis on press-pellet of the same sample by PXRF (see text for more details and table A5 for the other elements) with associated uncertainties.

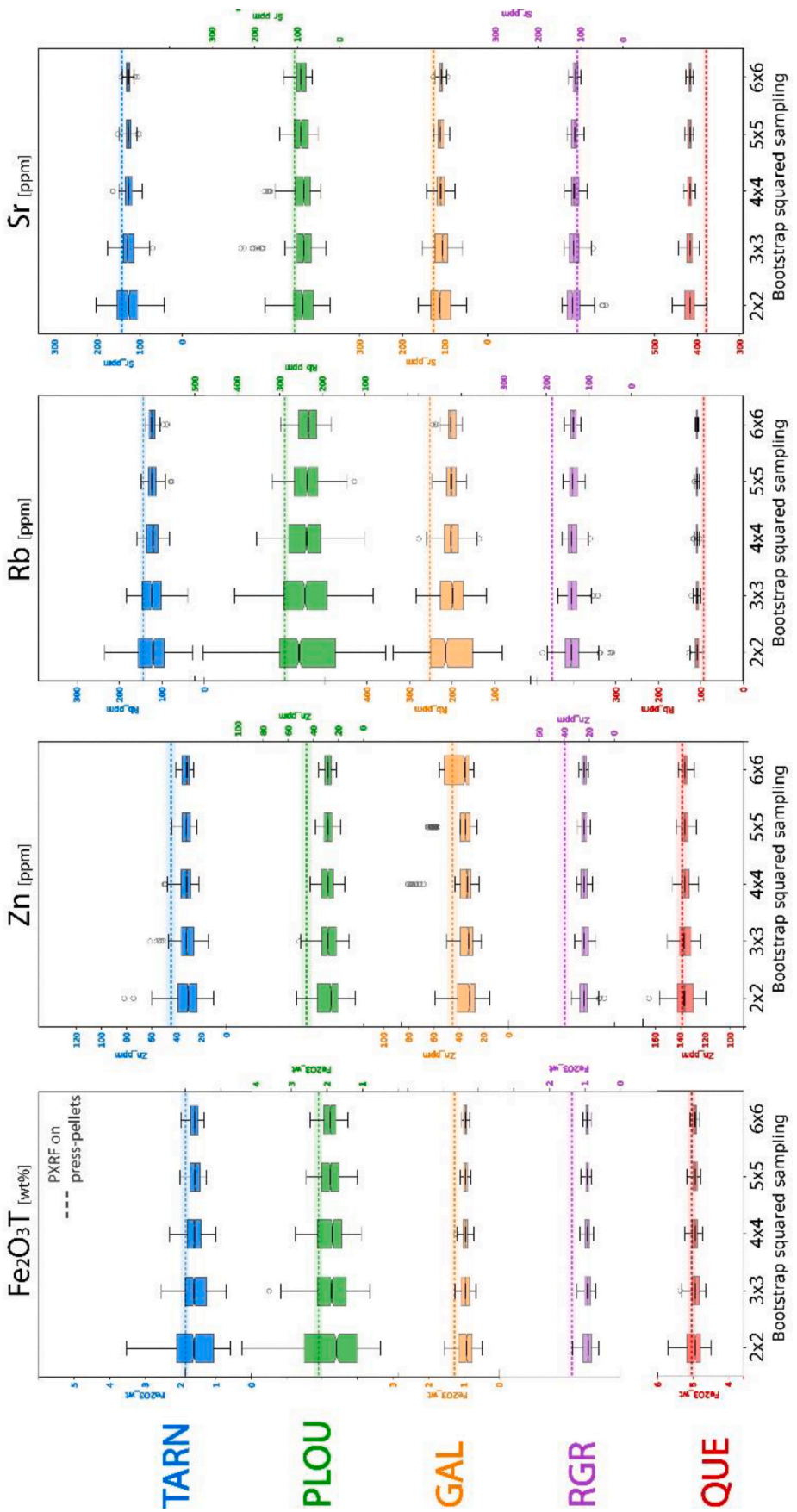

Fig. 6. (*continued*).

3 × 3 and the TARN sample) and compared to lab WDS-XRF value (see red line). As expected, it shows that using a continuous grid approach (Fig. 5b) minimizes the spread of the distribution of mean values, as shown by the difference between quantile values of the distribution (qdiff = 0.75 quantile – 0.25 quantile; qdiff = 2.08 *vs.* 1.68 for random *vs.* grid averaged analyses; see black dashed lines in Fig. 5 d-f). This approach also provides the estimation closer to the reference value (Fig. 5e). Averaging each grid's spectra before quantifying mass fractions systematically leads to an over-estimation of expected concentrations for most of the elements (Fig. 5f), probably due to an enhanced peak-background ratio for merged spectra that will affect the quantification/calibration process.

The effect of the subsampling grid size is shown in Fig. 6 for eight major and trace elements (Si, Ca, Ti, K, Fe, Zn, Rb, Sr) and for each granitoid sample. These patterns compared to PXRF analyses obtained on press-pellets (very fine-grained by definition) of the same sample. As expected, larger subsampling grid size leads to better reproducibility of element concentration (example for Ca content in TARN sample ranging from 1.61 ± 0.32 wt% to 1.62 ± 0.14 wt% CaO, for 2 × 2 to 6 × 6 grid size respectively; an example of the Sr content ranging from 127.9 ± 22.1 ppm to 127.4 ± 3.5 ppm Sr, for 2 × 2 to 6 × 6 grid size respectively). Samples with small grain sizes (like RGR or QUE) show a more clustered distribution even with 2 × 2 subsampling. These results show that the uncertainties are highly improved/minimized from 3 × 3 grid size for fine-grained samples (*i.e.*, RGR and QUE) and from 4 × 4 grid size for coarser-grained samples (*i.e.* TARN, PLOU, GAL; see Fig. 6) but then, do not improve significantly using larger grid sizes. These trends are displayed in Fig. 6 and, median values, boxplots boundaries and offset percentages for each element and each sample are provided in appendix A5. This bootstrap analysis is compared to chemical concentrations on press-pellets for each rock sample (Fig. 6 and appendix A6).

5. Portable magnetic susceptibility (pMS)

5.1. Instrument and operational conditions

A portable MS3 magnetic susceptibility meter (pMS; Bartington Ltd.) was used for this study, linked to the MS2K field sensor (from the Belgian Geological Survey, Belgium). The latter is made for measurements on a flat and smooth surface and has a surface of integration (spot size) of ca. 25.4 mm diameter. Changes in the amplitude of a low-frequency magnetic field measured by the MS3 with a magnetic susceptibility (MS) reach a resolution of 2 μSI (Deng, 2015). Each sample measurement was conducted as follows: ten successive analyses of a disk-shaped MS reference material were performed before each analysis sequence per sample. MS analyses of this reference material yield an averaged value of 4641 ± 39 μSI (standard deviation of 199; only 0.36% offset from manufacturer reference value). Then, ten successive analyses of the sample lasting 10 s each were bracketed by two 10 s analyses of blank (gun targeting the air) for instrument drift correction. All the reference material validation values and magnetic susceptibility results corrected from the instrumental blank can be found in Appendix A7.

5.2. Magnetic susceptibility of igneous rocks with different grain sizes

As for PXRF analysis, we performed 100 discrete analyses distributed on a 10 by 10 cm square grid (Fig. 7; see operational conditions described above). Bootstrap analysis using a similar procedure as in section 4.4 was conducted for each sample; by subsampling (respectively n = 2, 3, 4, 5, 6, 7, 8) the set of hundred analyses at each iteration averaging n by n numbers of individual analyses as a continuous square grid (see explanation in the previous section). As expected, increasing the size of the subsampling grid minimizes the spread of averaged values of magnetic susceptibility. TARN, PLOU and RGR granitoids show lower MS values ranging between 600 and 1000 μSI, while GAL and QUE are characterized by higher MS signatures, ranging from 4000 to 9500 μSI (Fig. 7). The spreading of averaged values is strongly minimized from 5 × 5 for the coarser-grained granitoids (TARN and PLOU) and 6 × 6 for

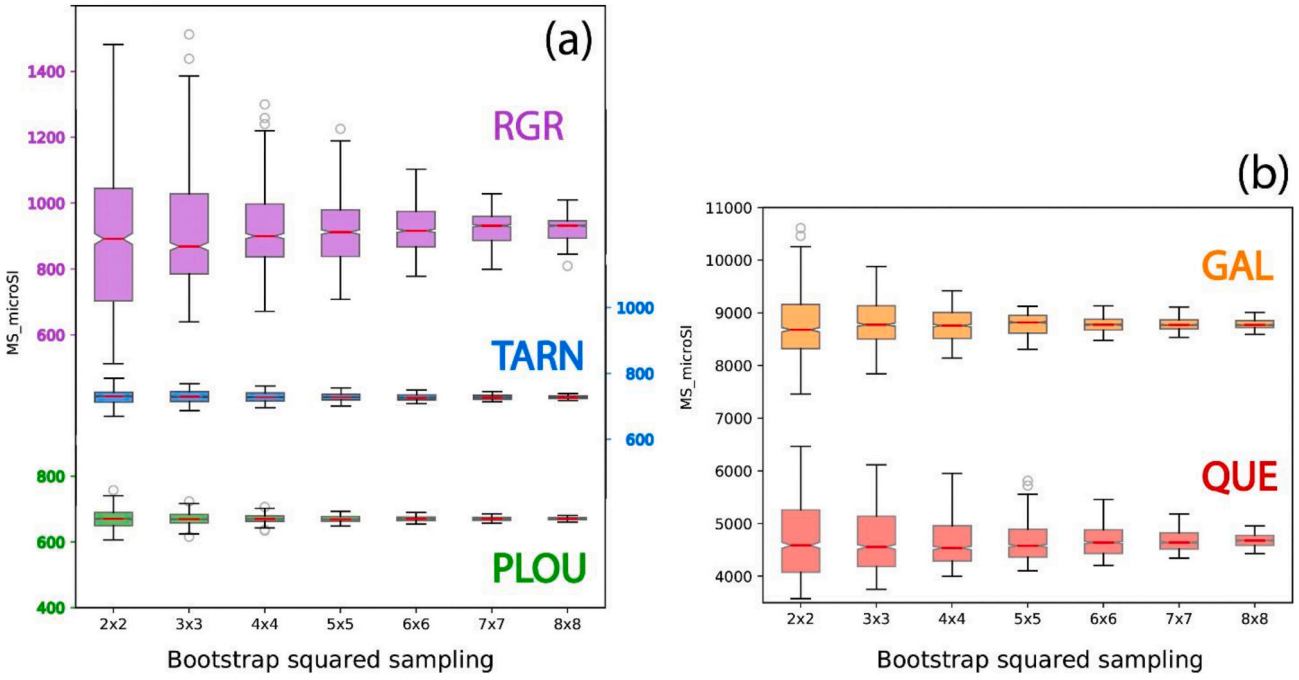

Fig. 7. Results of the bootstrapped Magnetic Susceptibility analysis applied to in house granitoid samples (in a similar manner as for pXRF analyses; see data table in appendix A7). Boxes extend from the lower to upper MS quartile values of each sampling size and the red line is for the median value. Black whiskers show the range of the dataset except for identified outliers in whitish symbols. (For interpretation of the references to color in this figure legend, the reader is referred to the Web version of this article.)

medium to fine-grained granitoids (GAL, RGR and QUE; see Fig. 7). Interestingly, the magnetic susceptibility values and the spread of their averaged value are less affected by the rocks' mean grain size than for PXRF analysis. This trend could partially be explained by the spotsize used for pMS analysis that is larger than for PXRF. However, the bootstrap analysis applied on pMS values on Fig. 7 shows that QUE sample (the fine-grained rock) displays a spread in pMS values that is more than twice larger than for the RGR sample (the coarse-grained rock) for a given squared sampling size. This means that the MS signal and its intensity rely more likely on the nature, *i.e.* the magnetic response, and the proportions of their constitutive mineral phases.

6. Application in geoarchaeology: provenance study of roman granitic quarries in southern corsica

Located in the Western Mediterranean region, Corsica formed with Sardinia, the European continent's margin, during the Mesozoic Tethys era. In Corsica, remnants of this lithological basement mainly crop out in the western and southern sides of the island (Fig. 8a) and is made of intermediate to felsic (and only a few mafic) igneous/plutonic rock units (referred to as "granitoids" hereafter). These granitoids were successively emplaced during the Carboniferous up to the Permian-Triassic transition (from ca. 305 to 260 Ma; Paquette et al., 2003; Cocherie et al., 2005). They show variable geochemical signatures, ranging from calc-alkaline to meta-aluminous alkaline composition, marking the transition from the pre-to post-collisional tectonics that formed the batholitic basement of the Corsica-Sardinia crustal block (Lardeaux et al., 1994; Ferré and Leake, 2001; Rossi et al., 2009). The Lavezzi archipelago is part of this batholith, located in southern Corsica in the Straits of Bonifacio. It is made of numerous major islands surrounded by small ones (Fig. 8b); three of these islands include from north to south: the Cavallo, San Bainzu and Lavezzu islands. The latter is mainly made of a medium to coarse-grained granitoid with numerous pluri-centimetric mafic enclaves. Southern Cavallo and San Bainzu islands are very similar to each other and were both geologically mapped as the same granodiorite as Lavezzu island (Orsini et al., 2011a, 2011b). The basement of the northern side of Cavallo island consists of a monzogranite to granodiorite (Fig. 8b). These granitoids units are

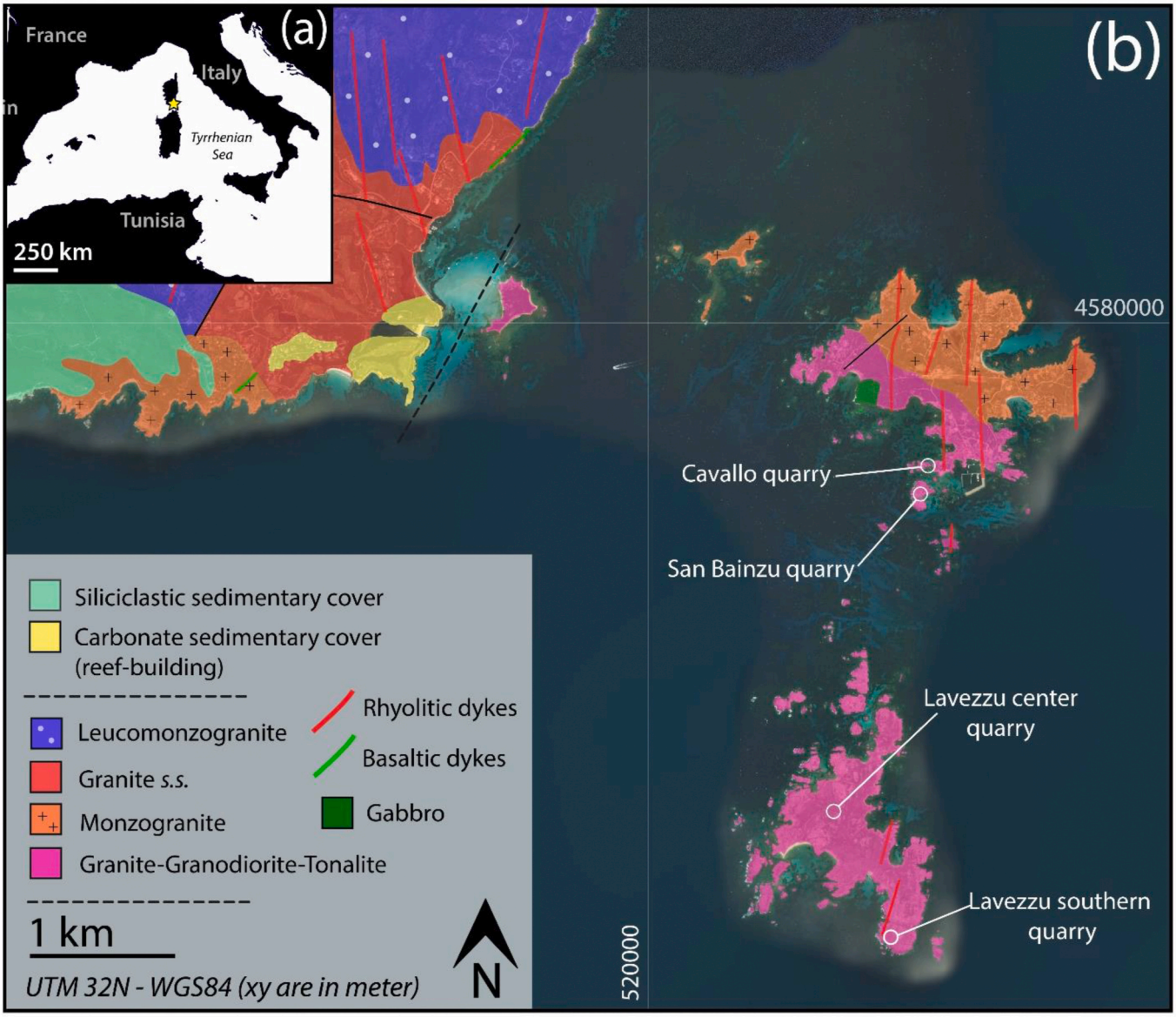

Fig. 8. Sketch of the geological map of the islands of the Lavezzi archipelago, including Cavallo, San Bainzu and Lavezzu islands (redrawn based on the BRGM geological map from Orsini et al., 2011a, 2011b). A georeferenced KMZ file of this map is available in the supplementary material B1, provided using the Geolokit app (Triantafyllou et al., 2017).

Fig. 9. Field pictures showing (a) quarried front of the southern Cavallo quarry being analyzed with PXRF instrument and (b) the Bonifacio column (War Memorial at the Bonifacio locality) that has been extracted from the San Bainzu quarry after World War I.

crosscut by pluri-metric, subvertical and N- to NNE-trending dykes of pink rhyolite in the islands.

The following sections aim to apply our multiple techniques characterization approach in the field at quarried sites on the Lavezzi archipelago and conduct a provenance study on a Roman column exposed as a War Memorial at the Bonifacio locality (Fig. 9b). This column was extracted with certainty from the San Bainzu quarry (Gauthier, 2017; Canonici, 2014; Clavel, 1924) and erected on the November 11, 1932 in Bonifacio (Pellegrinetti and Ravis-Giordani, 2010). We will use this column as a witness to test if our approach can discriminate different quarries' sources with an enhanced spatial resolution and for igneous rocks that appear to be very similar, even indistinguishable by human eyes in the field. The three quarried sites show similar morphological features. They consist of "open-pit" quarries, with a stepped profile consisting of working faces and stepped benches (Fig. 9a) with the quarry bed at the level of the bedrock (Clerbois et al., 2020). Constraining the estimation of extracted rock volumes in each quarry is still a work in progress (Clerbois et al., 2020). Bench sizes range between 5 and 30 m in length and 2–5 m in height and extracted columns ranging between 3 and 9 m long and around 0.5–1.5 m in diameter. The Bonifacio column (Fig. 9b) measures ca. 8.8 m long and with 3.8 of circumference (*i.e.* 5 m of the column is out of the ground at the moment and the rest underground to ensure monument stability).

Image analysis of each rock sample was applied following the same procedure described in section 3. Photographs were taken directly on the quarry's fronts; RAW images were corrected for brightness, white balance and scaled (10 cm side square) and ultimately, the image was segmented using the Weka ML algorithm for feldspar, quartz and ferromagnesian phases that are recognizable based on sample photographs. However, quartz and felspars can be challenging to discriminate, specifically when the rock surfaces are fresh and felspars tend to be greyish and translucid (instead of whitish when slightly weathered). Therefore, the proportions of melanocratic minerals (biotite + amphibole) and the ratio of proportions of melanocratic on leucocratic (quartz + feldspar) minerals are used as a discriminating parameter (referred respectively as xFeMg and M/L hereafter). Granodiorite rock from the Cavallo quarry shows the highest M/L ratio at 0.53 and high xFeMg (34.8 vol%). Granitic rock from the Lavezzu quarry shows the lowest M/L ratio with a value at 0.12 and low xFeMg at 11.0 vol%. San Bainzu quarry shows intermediate values ranging from 0.18 to 0.23 as well as for xFeMg values from 15.2 to 18.8 vol%. The granodiorite from the Bonifacio column shows an M/L value of 0.16 and xFeMg of 14.0 vol%. Results for each mineral phase proportion are summarized in appendix A8.

For magnetic susceptibility measurements, the protocol optimized in the lab was applied for each investigated rock from the quarrying site or monument. Respectively, three, five and three sampling sites were analyzed for south Cavallo, Lavezzu and San Bainzu quarries. Averaged pMS values between the same sampling sites show good reproducibility (Fig. 10). South Cavallo sampling site shows magnetic signature similar to San Bainzu sampling site, with weighted averages of 5254 ± 69 μSI and 5749 ± 67 μSI, respectively (uncertainty at 2σ; Fig. 10). Lavezzu sampling site shows a lower magnetic susceptibility value (with a weighted average at 3655 ± 34 μSI; Fig. 10). This MS shift between Lavezzu and San-Bainzu-Cavallo granitoids is in agreement with the laboratory MS analyses made in southern Corsica in Gattacceca et al. (2004). The MS analyses from the Bonifacio column monument show a weighted average of 5700 ± 92 μSI. This average value is closer to the San Bainzu MS signature but, considering the spread of the values, it cannot be distinguished from those from the southern Cavallo quarry (Fig. 10). The data table can be found in Appendix A9.

For PXRF analyses, the same protocol optimized in the lab was applied for each quarrying site or monument investigated. For each sampling site, a 4 × 4 cm grid was drawn in which sixteen regularly spaced PXRF analyses were performed. Each analysis was then processed through our in-house calibration using the CloudCal app. Each set of sixteen chemical concentrations data was then averaged to provide a representative value for the whole rock (error bars in Fig. 11 are 2 σ applied on the entire dataset). Two sites were analyzed in Cavallo and San Bainzu quarries and three sites in Lavezzu to check for good reproducibility of the method and its potential application as a high spatial resolution tracer. At first sight, chemical data of Cavallo and San Bainzu quarry sites are well clustered, while those from the Lavezzu quarry show larger variability between sampling areas (Fig. 11 a-e).

Based on specific chemical proxies, we precisely characterize the signature of rocks derived from the different quarries. Lavezzu quarried

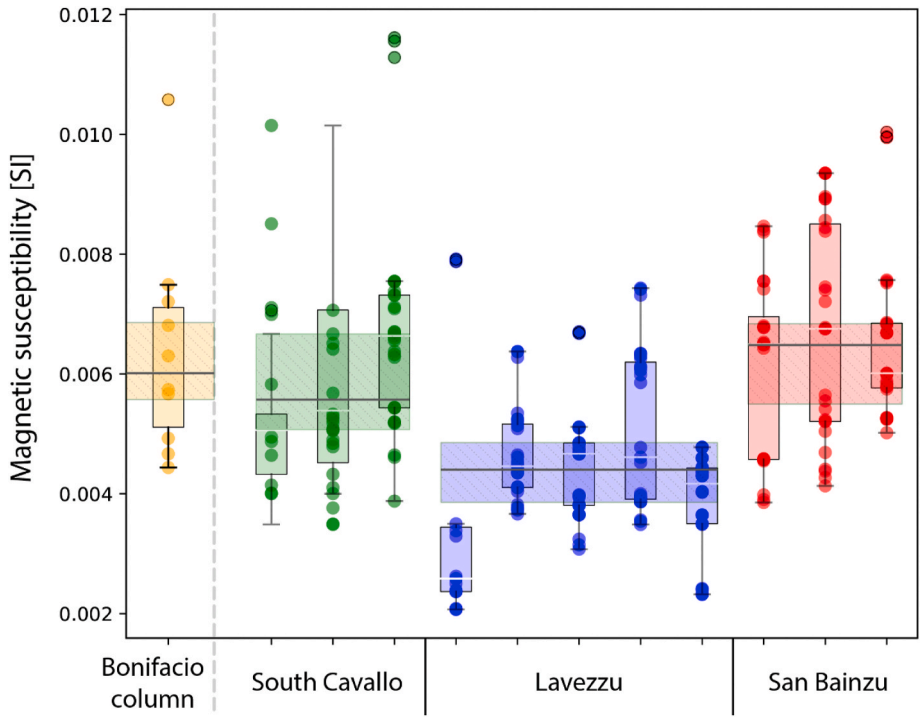

Fig. 10. Portable Magnetic Susceptibility (pMS) analyses of quarried sites (south Cavallo, south and central Lavezzu, San Bainzu) versus Bonifacio column monument. Boxes extend from the lower to upper MS quartile values of each sample and the white line is for the median value. Black whiskers show the range of the dataset. Large boxes and black horizontal lines show similar trend but integrating all the sample of each island.

rocks can clearly be distinguished from other quarried sites. Indeed, their chemical signature is marked by low CaO and Sr contents (<2 wt% and <210 ppm, respectively; Fig. 11 a and c) and slightly higher Si and Ba contents (>55 wt% and >400 ppm, respectively; Fig. 11 b and d) compared to other quarried rocks signature. These chemical proxies do not allow the discrimination between San Bainzu and southern Cavallo quarried rocks. However, K_2O and Rb contents are higher for San Bainzu granodiorite (>1.2 wt% K_2O and >75 ppm Rb) than for southern Cavallo granodiorite. A similar trend is observed for Fe and Ti contents, with higher values > 2 wt% Fe_2O_3T and >0.16 wt% TiO_2 for San Bainzu relative to the southern Cavallo rock samples (Fig. 11 a-d). A compilation of PXRF data can be found in Appendix A10.

7. Discussion

7.1. Defining PXRF applicability using the empirical limit of quantification (ELOQ)

The limit of quantification (LOQ) of a given element is defined as the lowest concentration that can be quantitatively detected with a stated accuracy and precision for this element. The LOQ will depend on several parameters, including the used illumination conditions, on the PXRF instrument's sensor but mostly on the method and quality of the in-house calibration. As factory calibrations of the Tracer IV PXRF instruments are designed for specific material matrix and generally less suitable for igneous rocks, we developed an in-house calibration method and determined its empirical LOQs (ELOQs) for each element. Limits of quantification are generally higher than the limit of detection (LOD) provided by the PXRF manufacturer but more informative for evaluating the confidence level for each analyzed chemical element. Therefore, we compared the PXRF compositional data obtained from our validation set of SRMs' press-pellets with their certified values by calculating their percentage of difference (PoD) defined as follows: PoD in % = *100 * abs [cy – Cy]/Cy*, where *cy* is the PXRF measured concentration for the *y* element while *Cy* is the certified reference concentration for the same element. The smaller the PoD value is, the better is the quantification of the chemical element. We compared the variation in PoD with its measured concentration (Fig. 12). These patterns generally define a power trendline, with an increase in PoD value for low concentrations. These trends allow to define an empirical estimation of the limit of quantification for each chemical element (Fig. 12). For our validation set of SRMs, some element concentrations were not low enough to involve an increasing trend of the PoD, preventing the estimation of their LOQ (these elements will be annotated with an asterisk hereafter). We defined three groups of chemical elements with their respective ELOQ in bracket: *(i)* PoD < 10% for Al_2O_3 (*), SiO_2 (*), K_2O (0.95 wt%), CaO (2.0 wt%), TiO_2 (0.4 wt%), Fe_2O_3 (1.8 wt%), Zn (25 ppm) and Sr (140 ppm); *(ii)* PoD comprised between 10 and 20% for MnO (*), Ga (17 ppm), Rb (20 ppm), Y (*), Zr (40 ppm), Nb (*) and Ba (150 ppm) and *(iii)* PoD > 20% or poorly quantified for MgO, As, Cu, V and Cr. ELOQs for chemical elements that are poorly calibrated are not specified. The latter should be avoided for quantification or rock discrimination purposes.

7.2. The applicability of PXRF measurements on coarse-grained igneous rocks

Our study showed that one should first evaluate the grain size of the rock sample qualitatively or quantitatively using image analysis to adapt the size of the pMS and PXRF analysis grid (see sections 3, 4.4 and 5.2). As an example, whole-rock chemistry of coarse-grained igneous rock (with an average grain size of ca. 10–30 mm^2; see Fig. 1) can thus be determined by averaging 16 individual analyses distributed within, e.g., 4 × 4 regular spaced grid (which takes about 18 min For the whole rock characterization). Rock with smaller grain size but visible individual grains (with average grain size 0.5–10 mm^2) could be determined by averaging nine individual analyses distributed as e.g., 3 × 3 regular spaced grid (which takes about 10 min For the whole rock characterization). To evaluate the applicability and the limitations of PXRF analysis on coarse-grained igneous rocks, we compared chemical compositions obtained: by laboratory techniques (WD-XRF, solution-ICP-

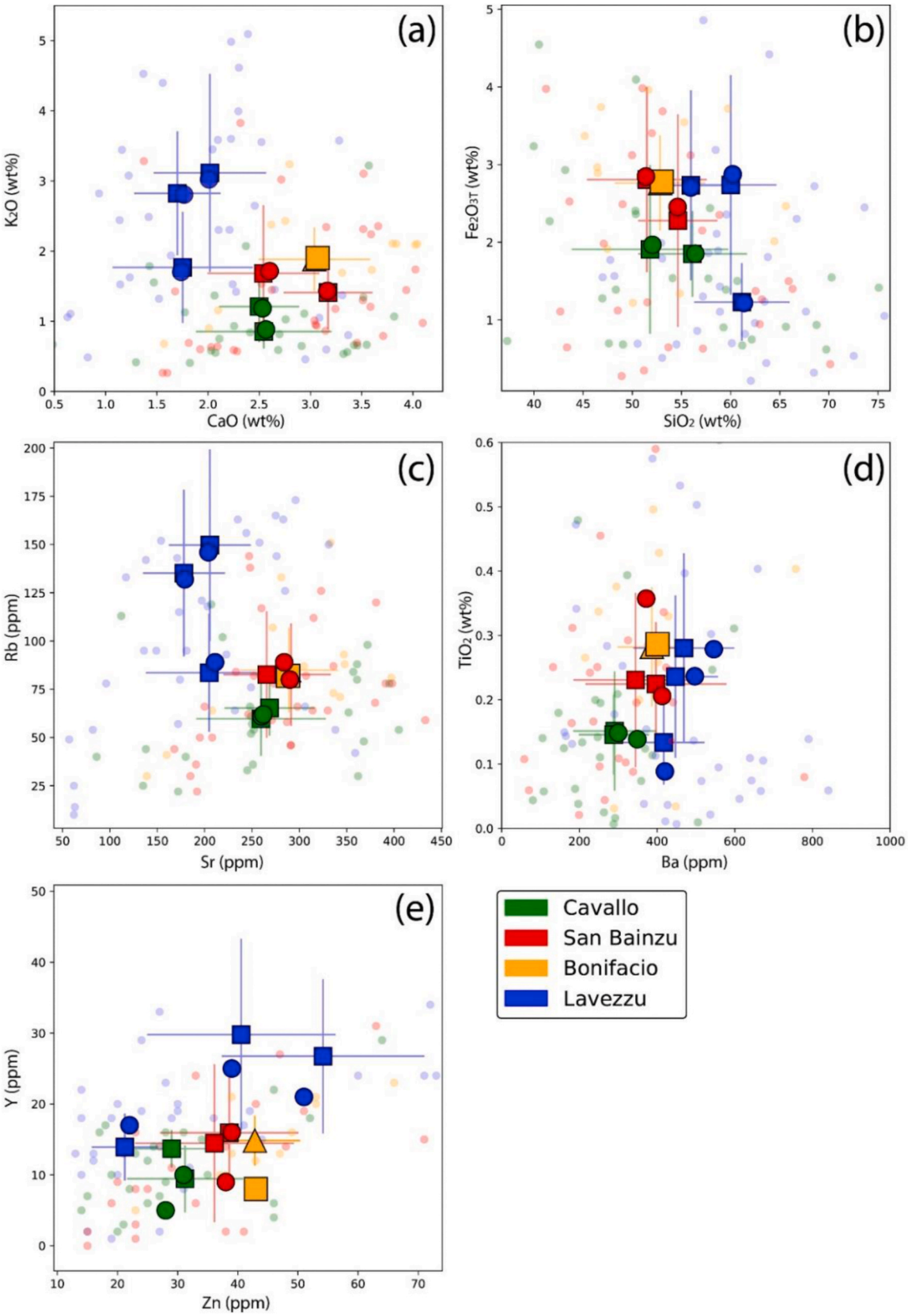

Fig. 11. a–e: Results of PXRF analyses of Corsican granitic rocks (quarried sites and the Bonifacio column) attesting the similarity between Bonifacio column and the San Bainzu quarries (using a 4 × 4 analyses grid). Square symbols are for average of individual analyses. Round and triangle symbols are for average of raw individual spectra. Error bars represent 2 sigma uncertainty. Small and faded circle symbols represent individual analyses.

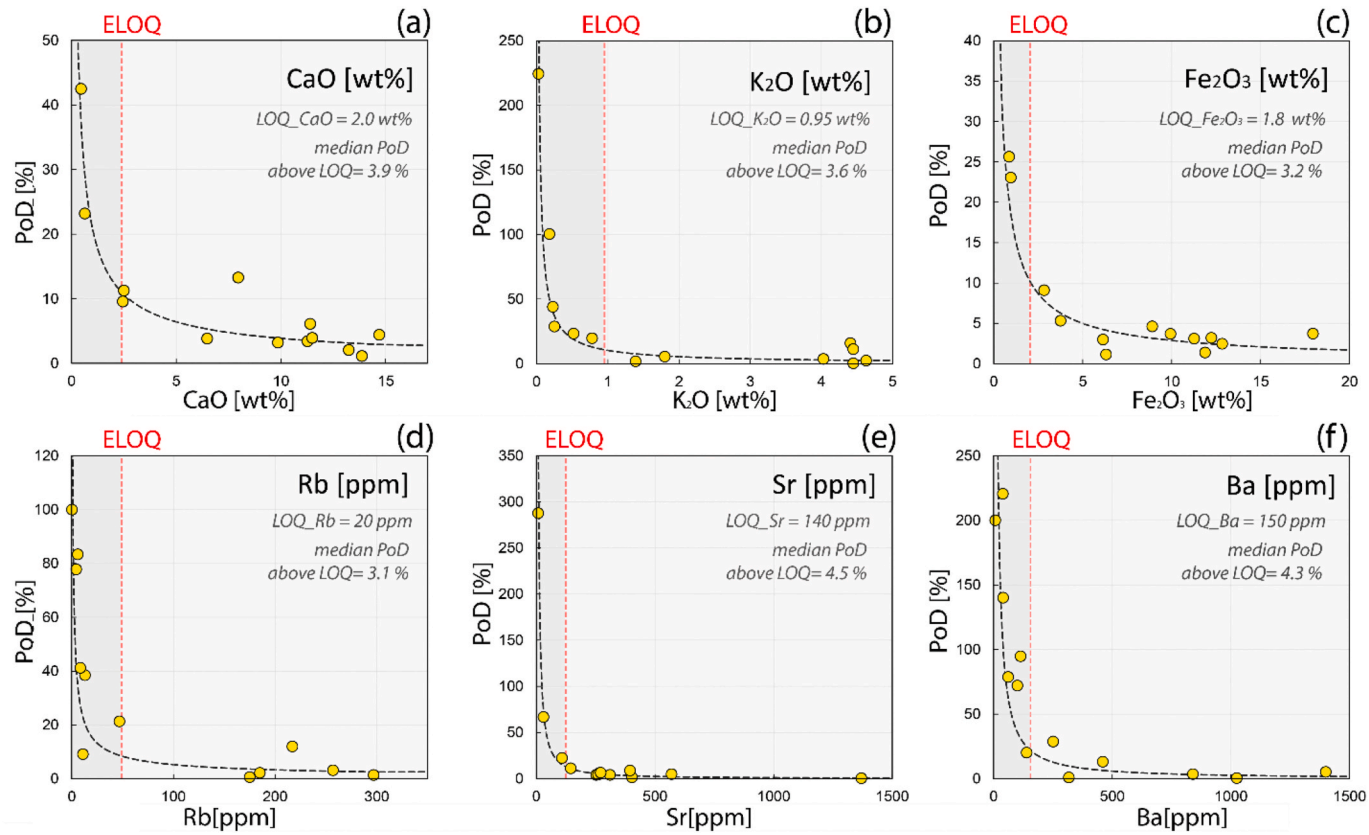

Fig. 12. Diagrams showing how Percentage of Difference (PoD) varies with measured concentrations of a given chemical element for some major (Ca, K, Fe) and trace elements (Rb, Sr, Ba). For a defined PoD range, the Limit of Quantification (LOQ) can thus be determined (see red dashed line). This LOQ value defines the low concentration limit under which our in-house calibration and PXRF configuration cannot provide an accurate result. (For interpretation of the references to color in this figure legend, the reader is referred to the Web version of this article.)

OES for major elements and solution-ICPMS for trace elements) with data acquired by PXRF instrument on finely powdered and homogeneous press-pellets and ultimately, those obtained on unprepared, coarse to fine-grained igneous rocks (Fig. 13 a-l). For the PXRF analysis of unprepared, coarse to fine-grained igneous rocks, the PoD of quantifiable elements is slightly higher in general than those obtained for press-pellets analyses. The PoD is still <10% for Al_2O_3, SiO_2, TiO_2, Sr between 10 and 20% for K_2O, CaO, Fe_2O_3, Zn, Ga, Rb, Y, Ba and higher than 20% for MgO, V, Cr, Mn, Cu, As, Zr, Nb. These results are illustrated in Fig. 13 and provide robust knowledge on which element can be used for rock discrimination taking into account its reproducibility in the targeted sample and its associated uncertainty.

In addition, we showed that for a given element, the relative variation of its concentration is relatively constant from one sample to another (Fig. 13), referring to PXRF or reference values. This indicates that PXRF analysis on unprepared coarse-grained can also be a valuable tool to constrain relative chemical variations at the scale of a sample and/or of an outcrop as well as to discriminate different clusters for geoarchaeological studies or linking rock sources and monuments characterized with the same instrument and analytical conditions. For field investigation, other effects should be taken into account, including the state of the rock surface, like moisture content, weathering degree and roughness of the surface, even if these aspects were discussed elsewhere (e.g., Kido et al., 2006; Forster et al., 2011; Hahn et al., 2020) but not along with the combined effect of coarse-grained materials.

7.3. Linking extraction and building sites using multiple proxies and optimized acquisition

The granitic column displayed in Bonifacio was extracted with absolute certainty from the San Bainzu roman quarry (see Gauthier, 2017; Clavel, 1924). Therefore, this monument can be used to apply and test our multiple method approach and establish if it helps discriminate different quarries' sources with an enhanced spatial resolution, specifically for igneous rocks that appear very similar in the field. We compared the quantified results gathered from pMS, PXRF and image analyses for the granite of the Bonifacio column with granitic sources from Cavallo, San Bainzu and Lavezzu quarries. Results from the Bonifacio column image analysis show significantly lower proportions of ferromagnesian phases and/or the M/L ratio (M/L < 0.23) than the Cavallo granitic source (M/L > 0.53) but relatively similar to San Bainzu and Lavezzu granitic rocks. The magnetic susceptibility (MS) signature of the Lavezzu granitic quarry shows a lower value (<3700 μSI) than other granitic samples (>5200 μSI; Fig. 10). This suggests that the Bonifacio column has not been extracted from the Lavezzu granitic quarry, but MS parameter cannot discriminate between Cavallo and San Bainzu quarrying sites. In contrast, based on PXRF chemical results, the granitic column from Bonifacio shows a chemical signature similar to the San Bainzu quarry (see Fig. 11). To quantify this apparent similarity, we calculated the percentage of difference (PoD; see section 7.1) between the chemical composition of the Bonifacio granitic column (set as the target sample) and the granitic samples from the Lavezzu, Cavallo and San Bainzu quarries (set as the unknowns). The PoDs of each chemical element are compared between each unknown site and displayed in Fig. 14c. We then calculated the proportion of minimal PoD for each unknown sites. The granitic rock from the San Bainzu quarry shows the highest proportion of minimal PoD with the granitic sample from the Bonifacio column (73.7% for San Bainzu quarry against 15.8% and 10.5% for Cavallo and Lavezzu quarries, respectively; Fig. 14a). We also applied the same approach, only considering well-quantified chemical

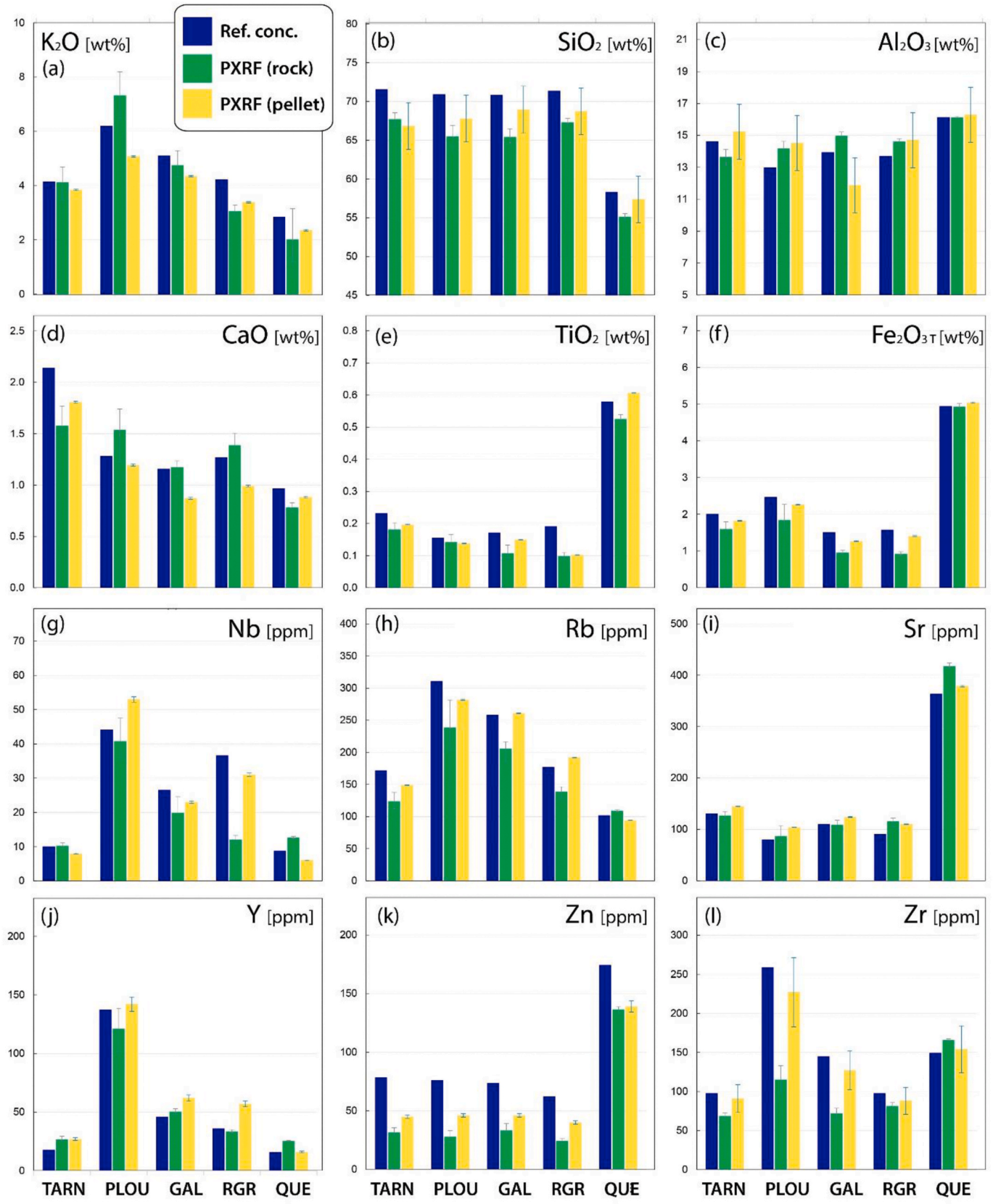

Fig. 13. Comparative histograms of composition in major and trace elements of the five granitoids, between "reference values" (from laboratory measurements: WD-XRF and solution-ICPMS) as blue bars and PXRF analyses on unprepared rock samples as green bars and on powdered press pellets as yellow bars. Samples from TARN to QUE are ordered from coarse to fine grained grainsize. Error bars represents 2 σ uncertainty. (For interpretation of the references to color in this figure legend, the reader is referred to the Web version of this article.)

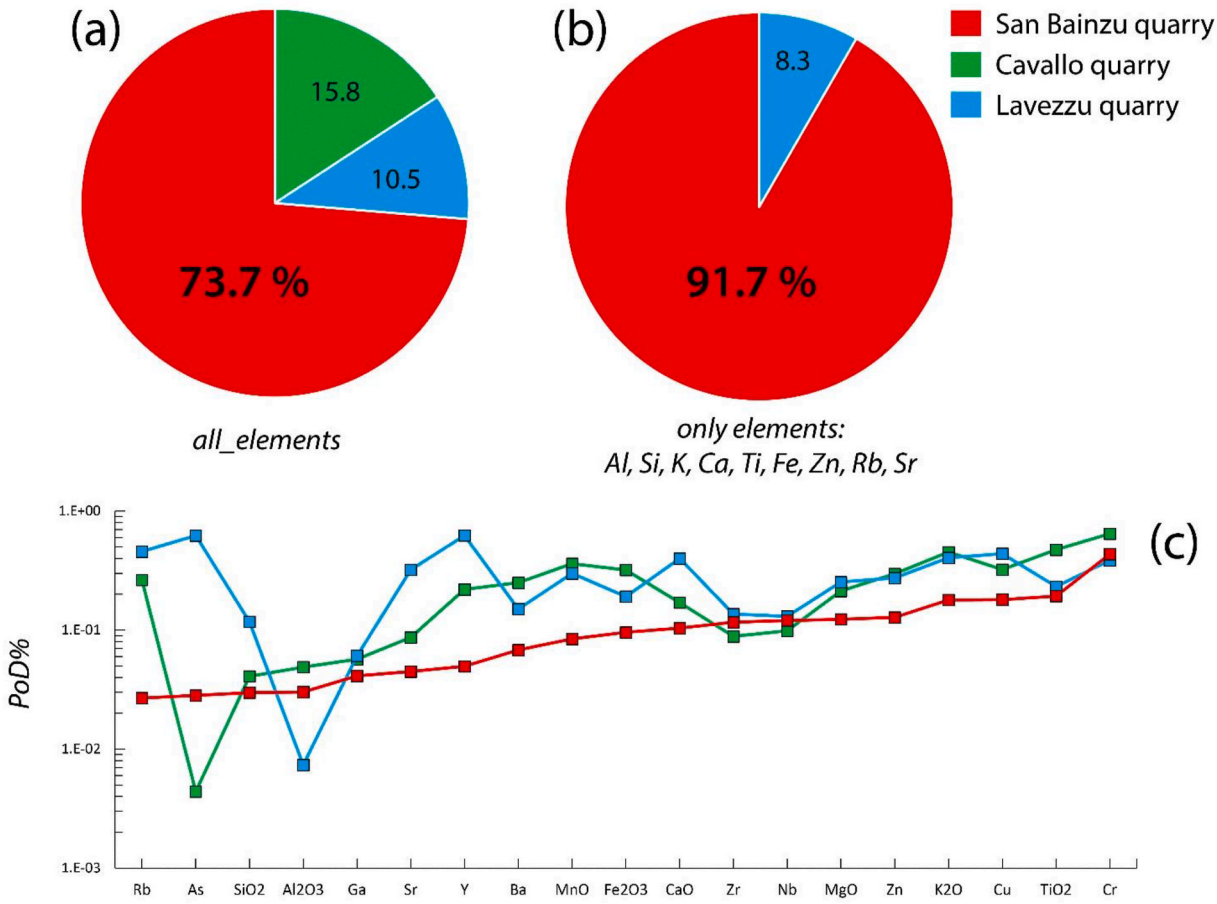

Fig. 14. Respective proportions of minimal Euclidian distance between Bonifacio column composition and potential source quarries (San Bainzu, Cavallo and Lavezzu) for (a) all calibrated chemical elements contents and (b) for the selection of discriminant chemical elements (Si, Al, K, Ca, Ti, Fe, Zn, Rb, Sr). The highest proportion is for San Bainzu quarry, suggesting it has the closest chemical signature to the targeted monument. (c) Multi-element diagram showing percentage of difference (PoD in %) between the Bonifacio column composition and potential source quarries for all quantified elements.

elements (as defined in sections 7.1 and 7.2: Al, Si, K, Ca, Ti, Fe, Zn, Rb and Sr). The San Bainzu granite yields the highest proportion of minimal PoD with the granitic rock from the Bonifacio column (91.7%; Fig. 14b). In other words, this proxy attests that from our method, the San Bainzu quarrying site shows the higher probability of being the source of the Bonifacio columnar monument, followed by the southern Cavallo and ultimately the Lavezzu quarrying sites but with low confidence. Our study demonstrates that combining non-invasive (PXRF, pMS and IA) characterization instruments with the textural and mineralogical observations determines local provenance at a high spatial resolution.

A multi-method approach is crucial for large scale geoarchaeological studies and provenance investigations of granitoids; more specifically for those exploited during the Roman period when a large variety of igneous rocks was extracted from a multitude of quarries scattered through the entire Roman empire (e.g., Turbay et al., 2019) and ultimately shaped for their monumental architecture. Although several major roman imperial projects were supplied by the mainstreamed *"Granito del Foro"* extracted from the *Mons Claudianus* quarry in the Eastern Desert of Egypt (e.g., Peacock et al., 1994), several authors emphasized the importance of alternative smaller quarrying spots providing a similar stylish igneous rock (e.g., Williams-Thorpe, 2008). Distinguishing between these rocks is delicate based on their appearance. Only a quantification of their mineralogical and geochemical composition could provide robust arguments to their identification and to apparent contradictions for the stone provenance, e.g. the provenance of granitic rocks used in the Baths of Caracalla, which are thought to be originated from Corsica (Williams-Thorpe et al., 1996) or ancient quarries in Turkey (Delaine, 1997).

A multi-method approach is critical for local to micro-regional studies, as illustrated by the study of the quarrying activity in the Lavezzi archipelago in the Strait of Bonifacio. As mentioned above, these islands display several quarrying sites, exploiting the same igneous batholith but at successive periods of time. Indeed, an important quarrying activity is attested during the Roman period (Clerbois et al., 2020) to produce large pieces, most likely sent overseas. An attested recent perturbation/activity (19th century) of these quarries provided rock blocks for local monuments (cemetery) or utility constructions (lighting, etc.). Our approach could precisely establish the links between the quarries and these recent local monuments or constructions in order to constrain the successive phases of rock exploitations better, the actual volume of rock extracted during each period of activity and ultimately, to constrain former vectors of commercial trades of granitic rock in global scenarios.

8. Conclusion and perspectives

This study explored the combined use of image analysis, pMS and PXRF, for characterizing coarse-grained igneous rocks. We provided a workflow for the users to optimize the use of these instruments, from their calibration method to their operational deployment in the field. Such a non-invasive multi-method approach re-opens the door to provenance studies of igneous materials with source identification at high spatial resolution in archaeometry. Statistical tools, including minimal PoD or principal component analysis (PCA; see examples in

Müskens et al., 2018), and established multivariate methods, such as K-Nearest Neighbors or Discriminant Function Analysis could be applied to this catalog to identify rock clusters and discriminate them by providing a percentage of confidence when comparing monuments and their potential quarry source. Future works aim to apply these methods on major monuments of the imperial era and Roman granitoids quarries exposed in the Tyrrhenian sea and compare their respective signatures for provenance identification.

Several developments should be considered as future directions. Concerning PXRF analysis, further research would optimize the combination of variable voltage conditions of the PXRF X-ray source and their respective acquisition times, using filters to enhance the signal on given chemical elements but adapting their use for field investigation and relatively fast analysis. During field investigation, other effects could be better constrained, as amongst others, the rock surface state, including its moisture content, the effect of rugged and irregular surface. Even if these aspects were discussed elsewhere (e.g., Kido et al., 2006; Forster et al., 2011; Hahn et al., 2020), their combined effects with coarse-grained materials remain poorly documented. These developments should be conducted on different types and models of PXRF instruments to provide comparable results between different studies. All these aspects are also of great importance for the PXRF embedded in future rover missions (Young et al., 2016) and the analysis of coarse-grained rocks during future planetary surface exploration.

Future directions also concern the testing, the development of calibration and optimization of other non-invasive, handheld instruments, including portable Raman spectrometer, recent Gamma-ray spectrometer, and portable Laser Induced Breakdown Spectroscopy (pLIBS). For the geoarchaeological community, the explosion and diversification of various spectroscopic data require the implementation of an integrated, collaborative, and open-access database to characterize archeological materials. In the same vein, several initiatives exist (e.g., see the IsoArch project for isotopic data; Salesse et al., 2018) and constitute a crucial opportunity to extent local investigations to a larger scale and identify systematics during past commercial trades at the scale of an established empire.

Acknowledgments

The first author (A.T) was an FRS-FNRS post-doctoral research fellow for the PROBARC project (Grant CR n°1. B. 414.20 F) during the conception and writing of this manuscript. NM and AT were supported by the F.R.S.-FNRS research credit CDR/OL J.0150.20. AC. Da Silva thanks Liege university for the support “Equipement 2018” for its support on the project « XRF Portable - geochemistry as a climatic proxy in paleo-records.» P. Kaskes thanks Research Foundation Flanders (FWO) for the awarded Ph.D. Fellowship (projects 11E6619N, 11E6621N). Ph. Claeys thanks the Research Foundation Flanders (Hercules) for purchasing the PXRF. This research is authorized and subsidized by the Regional Service of Archaeology (SRA) directed by Laurent Sévègnes of the Regional Direction of Cultural Affairs of Corsica (DRAC), directed by Franck Leandri within the annual archeological program. This work is part of the Collective Research Program on *“Les Bouches de Bonifacio à l’Epoque romaine: approches archéologique et géoarchéologique*". This project brings together about twenty researchers from five institutions (Centre Camille Jullian-CNRS, CEREGE-CNRS, *CReA Patrimoine/Université libre de Bruxelles*, DRASSM, INRAP). The program is facilitated by the logistical support of the Heritage Department of the Bonifacio Town Hall headed by Mrs. Hélène Portafax and has received financial assistance from ARPAMED fund (Archaeology and Heritage in the Mediterranean). The authors thank A. McAlister and two anonymous reviewers for their constructive comments on this manuscript and R. Torrence for the editorial handling.

Appendix A. Supplementary data

Supplementary data associated with this article can be found, in the online version, at https://doi.org/10.1016/j.jas.2021.105376.

References

Adam, J.-P., 2011. Roman Building: Materials and Techniques, 6e éd. Matériaux et techniques, Paris.
Arganda-Carreras, I., Kaynig, V., Rueden, C., Eliceiri, K.W., Schindelin, J., Cardona, A., Sebastian Seung, H., 2017. Trainable Weka Segmentation: a machine learning tool for microscopy pixel classification. Bioinformatics 33 (15), 2424–2426.
Baziotis, I., Xydous, S., Manimanaki, S., Liritzis, I., 2020. An integrated method for ceramic characterization: a case study from the newly excavated Kastrouli site (Late Helladic). J. Cult. Herit. 42, 274–279.
Bersani, D., Lottici, P.P., 2016. Raman spectroscopy of minerals and mineral pigments in archaeometry. J. Raman Spectrosc. 47 (5), 499–530.
Bersani, D., Madariaga, J.M., 2012. Applications of Raman spectroscopy in art and archaeology. J. Raman Spectrosc. 43 (11), 1523–1528.
Bonizzoni, L., Galli, A., Gondola, M., Martini, M., 2013. Comparison between XRF, TXRF, and PXRF analyses for provenance classification of archaeological bricks. X Ray Spectrom. 42 (4), 262–267.
Boulvain, F., Poulain, G., Tourneur, F., Yans, J., 2020. Potential discrimination of Belgian black marbles using petrography, magnetic susceptibility and geochemistry. Archaeometry 62 (3), 469–492.
Burke, A.L., 2018. Chert, silex, and obsidian sourcing. The Encyclopedia of Archaeological Sciences 1–5.
Clavel, A., 1924. La carrière romaine de San Bainzu. Rev Corse 29, 156.
Clerbois, et al., 2020. The Roman Granite Quarries in the Tyrrhenian Sea during the Imperial Period: a Technological Study. in press. Marmora, (in press).
Clinton, C.K., Duncan, C.M., Shaw, R.K., Jackson, L., Jackson, F.L., 2019. Identification of trace metals and potential anthropogenic influences on the historic New York African Burial Ground population: a pXRF technology approach. Sci. Rep. 9 (1), 1–10.
Craig, N., Speakman, R.J., Popelka-Filcoff, R.S., Glascock, M.D., Robertson, J.D., Shackley, M.S., Aldenderfer, M.S., 2007. Comparison of XRF and PXRF for analysis of archaeological obsidian from southern Peru. J. Archaeol. Sci. 34 (12), 2012–2024.
de Winter, N.J., Sinnesael, M., Makarona, C., Vansteenberge, S., Claeys, P., 2017. Trace element analyses of carbonates using portable and micro-X-ray fluorescence: performance and optimization of measurement parameters and strategies. J. Anal. Atomic Spectrom. 32 (6), 1211–1223.
Delaine, J., 1997. The baths of Caracalla, A study in the design, construction, and economics of large-scale building projects in imperial Rome. JAT, Suppl. 25. Portsmouth, Rhode Island.
Deng, D.N., 2015. A Comparative Study of Handheld Magnetic Susceptibility Instruments. Doctoral dissertation, Laurentian University of Sudbury.
Drake, B., 2019. CloudCal v3.0. GitHub. https://doi.org/10.5281/zenodo.2596154.
Edwards, P.H., 2018. In-situ Spectroscopy on Mars: ChemCam Activities and Preparations for the Raman Laser Spectrometer on ExoMars. Doctoral dissertation, University of Leicester.
Eramo, G., Mangone, A., 2020. 14 Archaeometry of ceramic materials. Chem. Anal. Cult. Heritage 331.
Fabre, C., 2020. Advances in Laser-Induced Breakdown Spectroscopy Analysis for Geology: A Critical Review. Spectrochimica Acta Part B: Atomic Spectroscopy, p. 105799.
Fantuzzi, L., Kiriatzi, E., Romero, A.M.S., Müller, N.S., Williams, C.K., 2020. Punic amphorae found at Corinth: provenance analysis and implications for the study of long-distance salt fish trade in the Classical period. Archaeol. Anthropol. Sci. 12 (8), 1–21.
Ferré, E.C., Leake, B.E., 2001. Geodynamic significance of early orogenic high-K crustal and mantle melts: example of the Corsica Batholith. Lithos 59 (1–2), 47–67.
Forster, N., Grave, P., Vickery, N., Kealhofer, L., 2011. Non-destructive analysis using PXRF: methodology and application to archaeological ceramics. X Ray Spectrom. 40 (5), 389–398.
Galetti, G., Lazzarini, L., Maggetti, M., 1992. A first characterization of the most important granites used in antiquity. Ancient Stones: Quarrying, Trade and Provenance-Interdisciplinary Studies on Stones and Stone Technology in Europe and Near East from the Prehistoric to the Early Christian Period, pp. 167–177.
Gattacceca, J., Orsini, J.B., Bellot, J.P., Henry, B., Rochette, P., Rossi, P., Cherchi, G., 2004. Magnetic fabric of granitoids from southern corsica and northern Sardinia and implications for late hercynian tectonic setting. J. Geol. Soc. 161 (2), 277–289.
Gauthier, A., 2017. L’île de Cavallo dans l’archipel des Lavezzi (Corse): géologie, géomorphologie et exploitation des granites. Ecol. Mediterr. 43 (2), 23–33.
Germinario, L., Hanchar, J.M., Sassi, R., Maritan, L., Cossio, R., Borghi, A., Mazzoli, C., 2018. Trachyte of the Euganean Hills (NE Italy): New Petrographic and Geochemical Tracers for Recognizing Provenance Quarry in Archaeometry.
Hahn, A., Bowen, M.G., Clift, P.D., Kulhanek, D.K., Lyle, M.W., 2020. Testing the analytical performance of handheld XRF using marine sediments of IODP Expedition 355. Geol. Mag. 157 (6), 956–960.
Hall, G.E., Bonham-Carter, G.F., Buchar, A., 2014. Evaluation of portable X-ray fluorescence (pXRF) in exploration and mining: phase 1, control reference materials. Geochem. Explor. Environ. Anal. 14 (2), 99–123.
Hunt, A.M., Speakman, R.J., 2015. Portable XRF analysis of archaeological sediments and ceramics. J. Archaeol. Sci. 53, 626–638.

Jochum, K.P., Nohl, U., Herwig, K., Lammel, E., Stoll, B., Hofmann, A.W., 2005. GeoReM: a new geochemical database for reference materials and isotopic standards. Geostand. Geoanal. Res. 29 (3), 333–338.
Jochum, K.P., Nohl, U., Schwager, B., Stoll, B., Suesser, P., Weis, U., 2014. Geostandards and geoanalytical research bibliographic review 2013. Geostand. Geoanal. Res. 38 (4), 513–515.
Karydas, A.G., 2007. Application of a portable XRF spectrometer for the non-invasive analysis of museum metal artefacts. Ann. Chim.: J. Anal. Environ. Cult. Heritage Chem. 97 (7), 419–432.
Kasztovszky, Z., Maróti, B., Harsányi, I., Párkányi, D., Szilágyi, V., 2018. A comparative study of PGAA and portable XRF used for non-destructive provenancing archaeological obsidian. Quat. Int. 468, 179–189.
Killick, D., Stephens, J.A., Fenn, T.R., 2020. Geological constraints on the use of lead isotopes for provenance in archaeometallurgy. Archaeometry 62, 86–105.
Lardeaux, J.M., Menot, R.P., Orsini, J.B., Rossi, P., Naud, G., Libourel, G., 1994. Corsica and Sardinia in the variscan chain. Pre-Mesozoic Geology in France and Related Areas. Springer, Berlin, Heidelberg, pp. 467–479.
Launeau, P., Bouchez, J.L., Benn, K., 1990. Shape preferred orientation of object populations: automatic analysis of digitized images. Tectonophysics 180 (2–4), 201–211.
Lemiere, B., 2018. A review of pXRF (field portable X-ray fluorescence) applications for applied geochemistry. J. Geochem. Explor. 188, 350–363.
Liritzis, I., Zacharias, N., 2011. Portable XRF of archaeological artifacts: current research, potentials and limitations. X-ray Fluorescence Spectrometry (XRF) in Geoarchaeology. Springer, New York, NY, pp. 109–142.
Liritzis, I., Laskaris, N., Vafiadou, A., Karapanagiotis, I., Volonakis, P., Papageorgopoulou, C., Bratitsi, M., 2020. Archaeometry: an overview. Sci. Cult. 6 (1), 49–99.
Mathur, R., Burns, J., Powell, W., Boryk, R., Sheetz, B., D'Amico, P., Harney, P., 2020. Evaluation of Fe isotope values as a provenance tool for chert artefacts from the north-eastern United States. Archaeometry.
Müskens, S., Braekmans, D., Versluys, M.J., Degryse, P., 2018. Egyptian sculptures from Imperial Rome. Non-destructive characterization of granitoid statues through macroscopic methodologies and in situ XRF analysis. Archaeol. Anthropol. Sci. 10 (6), 1303–1318.
Orsini, J. Ferrandini, Ferrandini, M., Loÿe, M.-D., Guennoc, P., Pluquet, F., Oggiano, G., Cherchi, G., Aversano, A., Gattacceca, J., Thinon, I., Orrù, P., Puliga, G., Pintus, M., Ulzega, A., 2011a. – Carte géol. France (1/50 000), feuille Sotta – Bonifacio – Santa Teresa di Gallura (1127). Orléans: BRGM. Notice explicative par.
Orsini J.B., Capdevila R., Ferrandini M., Ferrandini J., Loÿe M.-D., Guennoc P., Pluquet F., Thinon I., Santiago M., Oggiano G., Cherchi G., Orrù P., Puliga G., Pintus M., Ulzega A., Gamisans J., Tramoni P., André J.-P., Galloni F., Münch P., Saint-Martin S., Alamy Z., Reynaud J.-Y., Tessier B. (2011b), 360 p.
Oyedotun, T.D.T., 2018. X-ray fluorescence (XRF) in the investigation of the composition of earth materials: a review and an overview. Geol. Ecol. Landsc. 2 (2), 148–154.
Papakosta, V., Lopez-Costas, O., Isaksson, S., 2020. Multi-method (FTIR, XRD, PXRF) Analysis of Ertebølle Pottery Ceramics from Scania, Southern Sweden. Archaeometry.
Peacock, D.P., Williams-Thorpe, O., Thorpe, R.S., Tindle, A.G., 1994. *Mons Claudianus* and the problem of the 'granito del foro': a geological and geochemical approach. Antiquity 68 (259), 209–230.
Pellegrinetti, J.-P., Ravis-Giordani, G., 2010. « *Les monuments aux morts de la première guerre mondiale en Corse* ». Cah. Méditerranée 81 (2010), 239–251.
Puccini, A., Xhixha, G., Cuccuru, S., Oggiano, G., Xhixha, M.K., Mantovani, F., Casini, L., 2014. Radiological characterization of granitoid outcrops and dimension stones of the Variscan Corsica-Sardinia Batholith. Environ. Earth Sci. 71 (1), 393–405.
Rogerio-Candelera, M.A., 2016. Digital image analysis-based strategies for quantitative monitoring of rock art sites. J. Archaeol. Sci.: Rep. 10, 864–870. https://doi.org/10.1016/j.jasrep.2016.06.041.
Rossi, P., Oggiano, G., Cocherie, A., 2009. A restored section of the "southern Variscan realm" across the Corsica–Sardinia microcontinent. Compt. Rendus Geosci. 341 (2–3), 224–238.
Salesse, K., Fernandes, R., de Rochefort, X., Brůžek, J., Castex, D., Dufour, É., 2018. IsoArcH.eu: an open-access and collaborative isotope database for bioarcheological samples from Graeco-Roman World and its margins. J. Archaeol. Sci.: Rep. 19, 1050–1055.
Sapkota, Y., Drake, B.L., McDonald, L.M., Griggs, T.C., Basden, T.J., 2020a. Elemental composition and moisture prediction in manure by portable X-ray fluorescence spectroscopy using random forest regression. J. Environ. Qual. 49 (2), 472–482.
Sapkota, Y., Drake, B.L., McDonald, L.M., Griggs, T.C., Basden, T.J., 2020b. Elemental composition and moisture prediction in manure by portable X-ray fluorescence spectroscopy using random forest regression. J. Environ. Qual. 49 (2), 472–482.
Schindelin, J., Arganda-Carreras, I., Frise, E., Kaynig, V., Longair, M., Pietzsch, T., Tinevez, J.Y., 2012. Fiji: an open-source platform for biological-image analysis. Nat. Methods 9 (7), 676–682.
Senesi, G.S., Manzini, D., De Pascale, O., 2018. Application of a laser-induced breakdown spectroscopy handheld instrument to the diagnostic analysis of stone monuments. Appl. Geochem. 96, 87–91.
Sinnesael, M., de Winter, N.J., Snoeck, C., Montanari, A., Claeys, P., 2018. An integrated pelagic carbonate multi-proxy study using portable X-ray fluorescence (pXRF): maastrichtian strata from the Bottaccione Gorge, Gubbio, Italy. Cretac. Res. 91, 20–32.
Steiner, A.E., Conrey, R.M., Wolff, J.A., 2017. PXRF calibrations for volcanic rocks and the application of in-field analysis to the geosciences. Chem. Geol. 453, 35–54.
Szakmány, G., Kasztovszky, Z., Szilágyi, V., Starnini, E., Friedel, O., Biró, K.T., 2011. Discrimination of prehistoric polished stone tools from Hungary with non-destructive chemical Prompt Gamma Activation Analyses (PGAA). Eur. J. Mineral 23 (6), 883–893.
Triantafyllou, A., Watlet, A., Bastin, C., 2017. Geolokit: an interactive tool for visualising and exploring geoscientific data in Google Earth. Int. J. Appl. Earth Obs. Geoinf. 62, 39–46.
Turbay, I., Martín, J.M., Carrasco, I., Fernández-Ugalde, A., Becerra, J., Ortiz, R., Ortiz, P., 2019. Quarry identification and characterization of 2nd century A.D. Roman granite columns from Ecija (Spain). Mediterranean Archaeol. Arch. 19 (3), 157–172.
Turner, A., Chan, C.C., Brown, M.T., 2018. Application of field-portable-XRF for the determination of trace elements in deciduous leaves from a mine-impacted region. Chemosphere 209, 928–934.
Vandenabeele, P., Donais, M.K., 2016. Mobile spectroscopic instrumentation in archaeometry research. Appl. Spectrosc. 70 (1), 27–41.
Vander Auwera, J., Namur, O., Dutrieux, A., Wilkinson, C.M., Ganerød, M., Coumont, V., Bolle, O., 2019. Mantle melting and magmatic processes under La Picada stratovolcano (CSVZ, Chile). J. Petrol. 60 (5), 907–944.
Waters, M.J., 2016. Reviving antiquity with granite: spolia and the development of Roman Renaissance architecture. Architect. Hist. 59, 149–179.
Williams-Thorpe, O., 2008. A thousand and one columns: observations on the roman granite trade in the Mediterranean area. Oxf. J. Archaeol. 27, 73–89. https://doi.org/10.1111/j.1468-0092.2007.00297.x.
Williams-Thorpe, O., Potts, P.J., 2002. Geochemical and magnetic provenancing of Roman granite columns from Andalucía and Extremadura, Spain. Oxf. J. Archaeol. 21 (2), 167–194. https://doi.org/10.1111/1468-0092.00156.
Williams-Thorpe, O., Potts, P.J., Webb, P.C., 1999. Field-portable non-destructive analysis of lithic archaeological samples by X-ray fluorescence instrumentation using a mercury iodide detector: comparison with wavelength-dispersive XRF and a case study in British stone axe provenancing. J. Archaeol. Sci. 26 (2), 215–237.
Williams-Thorpe, O., Jones, M.C., Tindle, A.G., Thorpe, R.S., 1996. Magnetic susceptibility variations at Mons Claudianus and in Roman columns: a method of provenancing to within a single quarry. Archaeometry 38 (1), 15–41.
Young, K.E., Evans, C.A., Hodges, K.V., Bleacher, J.E., Graff, T.G., 2016. A review of the handheld X-ray fluorescence spectrometer as a tool for field geologic investigations on Earth and in planetary surface exploration. Appl. Geochem. 72, 77–87.